

A comprehensive study of spike and slab shrinkage priors for structurally sparse Bayesian neural networks

Sanket Jantre¹, Shrijita Bhattacharya^{*1}, and Tapabrata Maiti¹

¹Department of Statistics and Probability, Michigan State University

Abstract

Network complexity and computational efficiency have become increasingly significant aspects of deep learning. Sparse deep learning addresses these challenges by recovering a sparse representation of the underlying target function by reducing heavily over-parameterized deep neural networks. Specifically, deep neural architectures compressed via structured sparsity (e.g. node sparsity) provide low latency inference, higher data throughput, and reduced energy consumption. In this paper, we explore two well-established shrinkage techniques, Lasso and Horseshoe, for model compression in Bayesian neural networks. To this end, we propose structurally sparse Bayesian neural networks which systematically prune excessive nodes with (i) Spike-and-Slab Group Lasso (SS-GL), and (ii) Spike-and-Slab Group Horseshoe (SS-GHS) priors, and develop computationally tractable variational inference including continuous relaxation of Bernoulli variables. We establish the contraction rates of the variational posterior of our proposed models as a function of the network topology, layer-wise node cardinalities, and bounds on the network weights. We empirically demonstrate the competitive performance of our models compared to the baseline models in prediction accuracy, model compression, and inference latency.

Keywords: Bayesian Neural Networks, Variational Inference, Spike-and-Slab Priors, Structured Sparsity, Model Compression, Posterior Consistency.

1 Introduction

Bayesian Neural Networks (BNNs) are recently receiving widespread attention due to their potential to provide improved predictions with quantified uncertainty and robustness (Wilson and Izmailov, 2020). In particular, BNNs impose priors on the network weights and infer their posterior distributions through the training data. The main hurdle for the BNNs is that the posterior inference over millions of parameters is computationally challenging. Even though Markov chain Monte Carlo (MCMC) sampling methods (ex. Hamiltonian Monte Carlo) are guaranteed to produce samples from the true posterior, their exorbitant computational complexity prohibits their use for modern BNNs (Izmailov et al., 2021). Alternatively, variational inference (VI) is computationally scalable to ultra high-dimensional machine learning models (Jordan et al., 1999; Blei et al., 2017; Blundell et al., 2015).

A plethora of works that have focused on sparse BNNs have done so in the context of edge selection (e.g., Polson and Ročková (2018), Chérief-Abdellatif (2020), Bai et al. (2020), Sun et al. (2021)). Weight pruning approaches although memory efficient, lead to unstructured sparsity in neural networks which insufficiently

*corresponding author

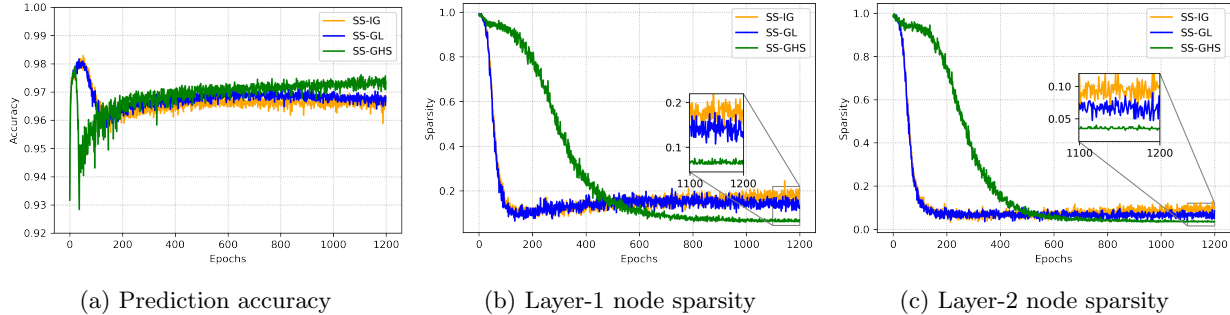


Figure 1: **MNIST Experiment.** Here, we demonstrate the performance of our SS-GL and SS-GHS models in a 2-layer perceptron network to classify MNIST, hand-written digits dataset. (a) we plot the classification accuracy on the test data for our models and include (Jantre et al., 2022)’s SS-IG model. (b) and (c) we plot the proportion of active nodes (node sparsity) in layer-1 and layer-2 of the network respectively. We observe that our SS-GHS yields the most compact network with the best classification accuracy.

reduce the computational cost during inference at test time. This is mainly because many of the dimensions of the weight matrices are not reduced even if most of the weights are zero (Wen et al., 2016). Instead, structured sparsity via node pruning - neurons in multilayer perceptrons (MLP) and channels in convolution neural networks (CNN), leads to lower computational cost at test-time due to reduced dimensions of weight matrices. Since our focus is to construct computationally compact networks, we focus on the task of node selection with the use of sparsity-inducing priors.

In the context of high dimensional linear regression, two of the most popular regularization techniques are lasso and horseshoe regularizers (Bhadra et al., 2019). Both Lasso and Horseshoe priors have been shown to outperform Gaussian priors in the context of Bayesian high dimensional linear regression. In this work, we employ the Lasso and Horseshoe-based regularization techniques for the task of neuron pruning. For an image classification experiment, Figure 1 demonstrates that spike-and-slab Group Lasso (SS-GL) and spike-and-slab Group Horseshoe (SS-GHS) exhibit an improvement over simple Gaussian prior in the slab part (SS-IG) in the context of a node selection. We used variational Bayes implementation.

We next discuss a few existing methods which perform the task of Bayesian node selection. Louizos et al. (2017) proposed the use of group normal Jeffrey’s prior and group Horseshoe prior for neuron pruning under VI framework. Ghosh et al. (2019) proposed to learn structurally sparse Bayesian neural networks through node selection with Horseshoe prior via variational inference. All these works use adhoc-thresholding techniques for neuron pruning and do not provide any theoretical validation. The current paper resolves both these issues (1) the use of a spike-and-slab prior with group-shrinkage slab distributions allows automated node selection (2) derivation of the convergence rates of the variational posterior provides theoretical justification.

Currently, there exists very little work on comparative analysis of the two shrinkage priors, Lasso and Horseshoe, even in the simple scenario of high dimensional Bayesian linear regression (see for e.g. Armagan et al. (2013)). To the best of our knowledge, there exists no work which does a thorough theoretical and numerical investigation of shrinkage priors like Lasso and Horseshoe in the context of variational Bayes neural networks.

1.1 Related Work

Sparse neural networks. A number of approaches to neural network compression via sparsity have been proposed in the literature (Cheng et al., 2018; Gale et al., 2019). Recent approaches (Guo et al., 2016;

Molchanov et al., 2017; Zhu and Gupta, 2018) in magnitude-based pruning of neural network weights provide high model compression rates with minimal accuracy loss. A key feature of sparsity in neural networks is its structure on the topology of the neural network weights. Although the unstructured weight pruning approaches (Han et al., 2015; Frankle and Carbin, 2019; Bai et al., 2020; Sun et al., 2021) lead to a lower memory footprint of the trained models, they are difficult to map to parallel processors and can incur computational overhead during inference. Instead, a structurally compact network can be obtained using node pruning approaches (Murray and Chiang, 2015; Alvarez and Salzmann, 2016; Ochiai et al., 2016; Liu et al., 2017; Luo et al., 2017; Louizos et al., 2018). Under the variational Bayesian framework, Louizos et al. (2017) and Ghosh et al. (2019) proposed to use continuous group shrinkage priors such as horseshoe priors on the entire parameters that selectively shrink the collection of weights associated with the nodes and prune those nodes using ad-hoc thresholding criteria.

Approximation theory. Schmidt-Hieber (2020) showed that estimators in nonparametric regression based on sparsely connected DNNs with ReLU activation function and wisely chosen architecture achieve the minimax estimation rates (up to logarithmic factors) under classical smoothness assumptions on the regression function. Their work forms a basis for the recent theoretical works on sparse neural networks involving weight pruning approaches under the Bayesian framework including Polson and Ročková (2018), and Sun et al. (2021). Chérief-Abdellatif (2020) and Bai et al. (2020) develop variational posterior consistency and its contraction rates for their spike-and-slab Gaussian priors in the context of edge selection.

1.2 Our Contributions

Firstly, structurally sparse Bayesian neural networks with shrinkage priors have not been explored from a theoretical point of view. Secondly, there does not exist any cohesive literature which establishes the theoretical and numerical efficiency of shrinkage priors over Gaussian prior in the slab part of spike-and-slab priors in the context of structurally sparse network training. Lastly, the theoretical and numerical properties of the corresponding variational implementation remain unexplored. To address these issues,

- We propose structurally sparse Bayesian neural networks using two distinct spike-and-slab prior setups, where the slab component uses hierarchical priors on the group of incoming weights (including bias) on the neurons: (i) **Spike-and-Slab Group Lasso (SS-GL)**, and (ii) **Spike-and-Slab Group HorseShoe (SS-GHS)**.
- We provide variational posterior consistency and optimal posterior contraction rates for our two proposed models with regularity assumptions on network topology. We also quantify the optimal choice of hyperparameters for variational posterior contraction.

2 Preliminaries

2.1 Bayesian Neural Networks

Let $Y \in \mathbb{R}$, $X \in \mathcal{X}$ be two random variables with the following conditional distribution

$$f_0(y|\mathbf{x}) = \exp [h_1(\eta_0(\mathbf{x}))y + h_2(\eta_0(\mathbf{x})) + h_3(y)] \quad (1)$$

where $\eta_0(\cdot) : \mathcal{X} \rightarrow \mathbb{R}$ is a continuous function satisfying certain regularity assumptions, \mathcal{X} is usually a compact subspace of \mathbb{R}^p and the functions h_1, h_2, h_3 are pre-determined. For $h_1(u) = u$, $h_2(u) = -\log(1 + e^u)$, $h_3(y) = 1$, we get the classification model. For $h_1(u) = u$, $h_2(u) = -u^2$, $h_3(y) = -y^2/2 - \log(2\pi)/2$, we get

the regression model with $\sigma^2 = 1$. Note, \mathbf{x} is a feature vector from the marginal distribution P_X and y is the corresponding output from $Y|X = \mathbf{x}$ in (1). Let $P_{X,Y}$ denote the joint distribution of (X, Y) .

Let $g : \mathcal{X} \rightarrow \mathbb{R}$ be a measurable function, the risk of g is $R(g) = \int_{\mathcal{Y} \times \mathcal{X}} \mathcal{L}(Y, g(X)) dP_{X,Y}$ for some loss function \mathcal{L} . The Bayes estimator minimizes this risk, Friedman et al. (2009). For regression with squared error loss and classification with 0-1 loss, the optimal Bayes estimators are $g^*(\mathbf{x}) = \eta_0(\mathbf{x})$ and $g^*(\mathbf{x}) = 1\{\eta_0(\mathbf{x}) \geq 0\}$ respectively. Practically, the Bayes estimator is not useful since the function $\eta_0(\mathbf{x})$ is unknown. Thus, an estimator is obtained based on the training observations, $\mathcal{D} = \{(\mathbf{x}_1, y_1), \dots, (\mathbf{x}_n, y_n)\}$. For a good estimator, the risk approaches Bayes risk as $n \rightarrow \infty$ irrespective of P_X . To this end, we use Bayesian neural networks, $\eta_{\boldsymbol{\theta}}(\mathbf{x})$ with $\boldsymbol{\theta}$ denoting the network weights, as an approximation to $\eta_0(\mathbf{x})$.

For $\mathbf{x} \in \mathbb{R}^p$, consider a BNN with L hidden layers, k_1, \dots, k_L number of nodes in the hidden layers, and $k_0 = p, k_{L+1} = 1$ (in regression). $k_{L+1} > 1$ allows the generalization to $Y \in \mathbb{R}^d, d > 1$, thereby providing a handle on multi class classification problems. The total number of parameters is $K = \prod_{l=0}^L k_{l+1}(k_l + 1)$. With $\mathbf{W}_l = [\mathbf{w}_l^0, \mathbf{W}_l^1]$, let

$$\eta_{\boldsymbol{\theta}}(\mathbf{x}) = \mathbf{w}_L^0 + \mathbf{W}_L^1 \psi(\mathbf{w}_{L-1}^0 + \mathbf{W}_{L-1}^1 \psi(\dots \psi(\mathbf{w}_1^0 + \mathbf{W}_1^1 \psi(\mathbf{w}_0^0 + \mathbf{W}_0^1 \mathbf{x}))), \quad (2)$$

where ψ is a nonlinear activation function, \mathbf{w}_l^0 are $k_{l+1} \times 1$ vectors and \mathbf{W}_l^1 are $k_{l+1} \times k_l$ matrices. Approximating $\eta_0(\mathbf{x})$ by $\eta_{\boldsymbol{\theta}}(\mathbf{x})$, conditional probabilities of $Y|X = \mathbf{x}$ are

$$f_{\boldsymbol{\theta}}(y|\mathbf{x}) = \exp[h_1(\eta_{\boldsymbol{\theta}}(\mathbf{x}))y + h_2(\eta_{\boldsymbol{\theta}}(\mathbf{x})) + h_3(y)]. \quad (3)$$

Thus, the likelihood function for the data \mathcal{D} under the model and the truth is

$$P_{\boldsymbol{\theta}}^n = \prod_{i=1}^n f_{\boldsymbol{\theta}}(y_i|\mathbf{x}_i), \quad P_0^n = \prod_{i=1}^n f_0(y_i|\mathbf{x}_i). \quad (4)$$

2.2 Variational Inference

We denote all the parameters of BNN with $\mathcal{T} = (\boldsymbol{\theta}, \boldsymbol{\omega})$, where $\boldsymbol{\omega}$ are the extra parameters beyond the network weights $\boldsymbol{\theta}$. The structure of the posterior distribution over \mathcal{T} is

$$\Pi(\mathcal{A}|\mathcal{D}) = \frac{\int_{\mathcal{A}} P_{\boldsymbol{\theta}}^n \pi(\mathcal{T}) d\mathcal{T}}{\int P_{\boldsymbol{\theta}}^n \pi(\mathcal{T}) d\mathcal{T}} = \frac{\int_{\mathcal{A}} P_{\boldsymbol{\theta}}^n \pi(\mathcal{T}) d\mathcal{T}}{m(\mathcal{D})} \quad (5)$$

where $P_{\boldsymbol{\theta}}^n = \prod_{i=1}^n f_{\boldsymbol{\theta}}(y_i|\mathbf{x}_i)$ is the likelihood function as in (4) and $\mathcal{A} \in \mathbb{T}$ where \mathbb{T} denotes the parameter space of \mathcal{T} . $\pi(\mathcal{T})$ denotes the joint prior density of $(\boldsymbol{\theta}, \boldsymbol{\omega})$, and $m(\mathcal{D})$ is the marginal density of the data which is free of the parameter set $(\boldsymbol{\theta}, \boldsymbol{\omega})$.

Let $\tilde{\pi}(\boldsymbol{\theta}) = \int_{\boldsymbol{\omega}} \pi(\boldsymbol{\theta}, \boldsymbol{\omega}) d\boldsymbol{\omega}$ be the marginal prior of $\boldsymbol{\theta}$ and $\tilde{\Pi}(\mathcal{A}) = \int_{\mathcal{A}} \tilde{\pi}(\boldsymbol{\theta}) d\boldsymbol{\theta}$ be the corresponding distribution function. The marginal posterior of $\boldsymbol{\theta}$ can be rewritten as

$$\tilde{\pi}(\boldsymbol{\theta}|\mathcal{D}) = \int \pi(\boldsymbol{\theta}, \boldsymbol{\omega}|\mathcal{D}) d\boldsymbol{\omega} = \frac{P_{\boldsymbol{\theta}}^n \tilde{\pi}(\boldsymbol{\theta})}{\int P_{\boldsymbol{\theta}}^n \tilde{\pi}(\boldsymbol{\theta}) d\boldsymbol{\theta}} = \frac{P_{\boldsymbol{\theta}}^n \tilde{\pi}(\boldsymbol{\theta})}{m(\mathcal{D})}$$

and let $\tilde{\Pi}(\mathcal{B}|\mathcal{D}) = \int_{\mathcal{B}} \tilde{\pi}(\boldsymbol{\theta}|\mathcal{D}) d\boldsymbol{\theta}$ be the probability distribution corresponding to $\tilde{\pi}(\boldsymbol{\theta}|\mathcal{D})$.

The posterior distribution in (5) is intractable and hence we employ variational inference to approximate it. Variational learning proceeds by inferring parameters of a distribution on the model parameters, q , by minimizing the Kullback-Leibler (KL) distance from the true Bayesian posterior, $\pi(\cdot|\mathcal{D})$, (Blei and Lafferty

(2007); Hinton and Van Camp (1993)):

$$\pi^* = \operatorname{argmin}_{q \in \mathcal{Q}} d_{\text{KL}}(q, \pi(\cdot|\mathcal{D})) \quad (6)$$

where $d_{\text{KL}}(\cdot, \cdot)$ denotes the KL-distance and \mathcal{Q} denotes the variational family. The variational family member q can be written as $q(\boldsymbol{\theta}, \boldsymbol{\omega}) = q(\boldsymbol{\theta}|\boldsymbol{\omega})q(\boldsymbol{\omega})$. Expanding (6),

$$\begin{aligned} \pi^* &= \operatorname{argmin}_{q \in \mathcal{Q}} \int \int \left[\log q(\boldsymbol{\theta}, \boldsymbol{\omega}) - \log \pi(\boldsymbol{\theta}, \boldsymbol{\omega}|\mathcal{D}) \right] q(\boldsymbol{\theta}, \boldsymbol{\omega}) d\boldsymbol{\theta} d\boldsymbol{\omega} \\ &= \operatorname{argmin}_{q \in \mathcal{Q}} \left(\int \int \left[\log q(\boldsymbol{\theta}, \boldsymbol{\omega}) - \log \pi(\boldsymbol{\theta}, \boldsymbol{\omega}, \mathcal{D}) \right] q(\boldsymbol{\theta}, \boldsymbol{\omega}) d\boldsymbol{\theta} + \log m(\mathcal{D}) \right) \\ &= \operatorname{argmin}_{q \in \mathcal{Q}} [-\text{ELBO}(q, \pi(\cdot|\mathcal{D}))] + \log m(\mathcal{D}) = \operatorname{argmax}_{q \in \mathcal{Q}} \text{ELBO}(q, \pi(\cdot|\mathcal{D})) \end{aligned}$$

where ELBO denotes evidence lower bound. Since $\log m(\mathcal{D})$ does not depend on q , it is dropped from the optimization problem. The negative of the ELBO (\mathcal{L}) is simplified as

$$\mathcal{L} = -\mathbb{E}_{q(\boldsymbol{\theta}, \boldsymbol{\omega})} [\log L(\boldsymbol{\theta})] + d_{\text{KL}}(q(\boldsymbol{\theta}, \boldsymbol{\omega}), \pi(\boldsymbol{\theta}, \boldsymbol{\omega})), \quad (7)$$

where $L(\boldsymbol{\theta})$ is the likelihood function of the data depending on the network weights $\boldsymbol{\theta}$.

Let $\tilde{\pi}^*(\boldsymbol{\theta}) = \int \pi^*(\boldsymbol{\theta}|\boldsymbol{\omega})\pi^*(\boldsymbol{\omega})d\boldsymbol{\omega}$, then $\tilde{\pi}^*$ denotes the marginal variational posterior for $\boldsymbol{\theta}$ and the corresponding probability distribution function is $\tilde{\Pi}^*(\mathcal{B}) = \int_{\mathcal{B}} \tilde{\pi}^*(\boldsymbol{\theta})d\boldsymbol{\theta}$.

3 Structured Sparsity: Spike-and-Slab Hierarchical Priors

In order to carry out automatic node selection to induce structured sparsity in BNNs, we consider spike-and-slab priors consisting of a Dirac spike (δ_0) at 0 and a uniform slab distribution elsewhere (Mitchell and Beauchamp, 1988). The spike part is represented by an indicator variable which is set to 0 if a node is not present in the network. Whereas, zero-mean Gaussian is the commonly used slab distribution in spike-and-slab priors (Jantre et al., 2022). However, their use can lead to inflated predictive uncertainties, especially when used in conjunction with fully factorized variational inference (Ghosh et al., 2019). Instead, if we consider a slab distribution having zero-mean Gaussian distribution with its scale being a random variable then the slab part of the marginal prior distribution will have heavier tails and higher mass at zero. Such hierarchical distributions in slab part further improve the sparsity as well as circumvent the inflated predictive uncertainties.

In the following subsections, for optimal layer-wise node selection, we make the prior inclusion probability λ_l depend on the layer index l . We shall assume a spike-and-slab prior and a corresponding spike-and-slab variational family.

3.1 Spike-and-slab group lasso (SS-GL):

Prior: Let z_{lj} be the indicator for the presence of j^{th} node in the l^{th} layer.

$$\begin{aligned} \pi(\bar{\boldsymbol{w}}_{lj}|z_{lj}) &= (1 - z_{lj})\boldsymbol{\delta}_0 + z_{lj}N(0, \sigma_0^2 \tau_{lj}^2 \mathbf{I}) \\ \pi(z_{lj}) &= \text{Ber}(\lambda_l), \pi(\tau_{lj}^2) = G(k_l/2 + 1, \varsigma^2/2) \end{aligned} \quad (8)$$

where $l = 0, \dots, L$, $j = 1, \dots, k_{l+1}$. Here, $N(\cdot, \cdot)$, $\text{Ber}(\cdot)$, and $G(\cdot, \cdot)$ represent Gaussian, Bernoulli, and Gamma distributions, $\bar{\boldsymbol{w}}_{lj} = (\bar{w}_{lj1}, \dots, \bar{w}_{lj k_{l+1}})$ is a vector of edges incident on the j^{th} node in the l^{th} layer,

δ_0 is a Dirac spike vector of dimension $k_l + 1$ with all zero entries and \mathbf{I} is identity matrix of dimension $k_l + 1 \times k_l + 1$. Assume all z_{lj} with $j = (1, \dots, k_{l+1})$ follow $\text{Ber}(\lambda_l)$ to allow for a common prior inclusion probability for all nodes in a layer l . Let $\lambda_L = 1$ to ensure no node selection occurs in the output layer. Finally, σ_0 and τ_{lj} are the constant global and variable local (per node) scale mixture components of the Gaussian slab. $\zeta^2/2$ is the constant rate hyperparameter of the Gamma distribution.

Variational family: We consider the following fully factorized variational family

$$\begin{aligned} q(\bar{\mathbf{w}}_{lj}|z_{lj}) &= (1 - z_{lj})\delta_0 + z_{lj}N(\boldsymbol{\mu}_{lj}, \text{diag}(\boldsymbol{\sigma}_{lj}^2)) \\ q(z_{lj}) &= \text{Ber}(\gamma_{lj}), \quad q(\tau_{lj}^2) = LN(\mu_{lj}^{\{\tau\}}, \sigma_{lj}^{\{\tau\}^2}) \end{aligned} \quad (9)$$

for $l = 0, \dots, L$, $j = 1, \dots, k_{l+1}$. Here $LN(., .)$ denotes Log-Normal distribution. The spike-and-slab structure of the variational family ensures that the variational weight distributions follow spike-and-slab structure allowing for exact node sparsity through variational approximation. Further, the weight distributions conditioned on the node indicator variables are all independent of each other. We use Log-Normal family instead of Gamma family to approximate Gamma distributed τ_{lj}^2 to facilitate numerical optimization. Additionally, $\boldsymbol{\mu}_{lj} = (\mu_{lj1}, \dots, \mu_{lj k_{l+1}})$ and $\boldsymbol{\sigma}_{lj}^2 = (\sigma_{lj1}^2, \dots, \sigma_{lj k_{l+1}}^2)$ be the variational mean and standard deviation parameters of the slab component of $q(\bar{\mathbf{w}}_{lj}|z_{lj})$. $\text{diag}(\boldsymbol{\sigma}_{lj}^2)$ is the diagonal matrix with $\sigma_{lj j'}^2$, being the j'^{th} diagonal entry. Here γ_{lj} denotes the variational inclusion probability for $q(z_{lj})$. Let $\gamma_{Lj} = 1$ to avoid node selection in output layer. Here $\mu_{lj}^{\{\tau\}}$ and $\sigma_{lj}^{\{\tau\}^2}$ are the variational mean and standard deviation of the Gaussian distribution of $q(\log \tau_{lj}^2)$.

ELBO: Let $\boldsymbol{\theta}$ be the network weights and $\boldsymbol{\omega} = (\mathbf{z}, \boldsymbol{\tau}^2)$ be the remaining parameters. We minimize the loss function: $\mathcal{L} = -\text{ELBO}(q(\boldsymbol{\theta}, \boldsymbol{\omega}), \pi(\boldsymbol{\theta}, \boldsymbol{\omega}|\mathcal{D}))$ where

$$\begin{aligned} \mathcal{L} = & -\mathbb{E}_{q(\boldsymbol{\theta}, \boldsymbol{\omega})}[\log L(\boldsymbol{\theta})] + \sum_{l,j} q(z_{lj} = 1) \int d_{\text{KL}}(N(\boldsymbol{\mu}_{lj}, \text{diag}(\boldsymbol{\sigma}_{lj}^2)), N(0, \sigma_0^2 \tau_{lj}^2 \mathbf{I})) q(\tau_{lj}^2) d\tau_{lj}^2 \\ & + \sum_{l,j} d_{\text{KL}}(\text{Ber}(\gamma_{lj}), \text{Ber}(\lambda_l)) + \sum_{l,j} d_{\text{KL}}(LN(\mu_{lj}^{\{\tau\}}, \sigma_{lj}^{\{\tau\}^2}), G(k_l/2 + 1, \zeta^2/2)) \end{aligned}$$

3.2 Spike-and-slab group horseshoe (SS-GHS):

Prior: We consider regularized version of group horseshoe (Piiironen and Vehtari, 2017) for the slab to circumvent the numerical stability issues of unregularized group horseshoe.

$$\begin{aligned} \pi(\bar{\mathbf{w}}_{lj}|z_{lj}) &= (1 - z_{lj})\delta_0 + z_{lj}N(0, \sigma_0^2 \tilde{\tau}_{lj}^2 s^2 \mathbf{I}), \quad \tilde{\tau}_{lj}^2 = (c^2 \tau_{lj}^2)(c^2 + \tau_{lj}^2 s^2)^{-1} \\ \pi(z_{lj}) &= \text{Ber}(\lambda_l), \quad \pi(\tau_{lj}) = C^+(0, 1), \quad \pi(s) = C^+(0, s_0) \end{aligned} \quad (10)$$

where $l = 0, \dots, L$, $j = 1, \dots, k_{l+1}$. Here, $C^+(., .)$ denotes half-Cauchy distribution. $\tilde{\tau}_{lj}^2$ is varying local (per node) scale parameter, s^2 is the varying global scale parameter, and σ_0^2 is constant global scale parameter. Here, s_0 is the scale parameter of half-Cauchy prior on s that can be tuned for specific situations. The prior inclusion probabilities, λ_l are common for all nodes from a given layer similar to SS-GL.

When weights are strongly shrinking towards 0, then $\tau_{lj}^2 s^2 \ll c^2$ and $\tilde{\tau}_{lj}^2 \rightarrow \tau_{lj}^2 s^2$ which leads to the unregularized version of the group horseshoe. When weights are away from 0, $\tau_{lj}^2 s^2$ will be large, i.e., $\tau_{lj}^2 s^2 \gg c^2$ and $\tilde{\tau}_{lj}^2 \rightarrow c^2$, where c^2 is constant. For these weights, the corresponding regularized group horseshoe in the slab follows $N(0, \sigma_0^2 c^2 \mathbf{I})$. This helps in thinning out the heavy tails of the horseshoe prior.

Instead of working with half-Cauchy distributions, we will employ a decomposition of the half-Cauchy that relies upon Gamma and Inverse Gamma distributions (Louizos et al., 2017) which allows us to compute the KL-divergence between scale prior $\pi(\tau)$ and the log-normal scale posterior $q(\tau)$ in closed form. A half-

Cauchy distribution can be reparameterized as $\tilde{\beta} \sim IG(1/2, 1)$, $\tilde{\alpha} \sim G(1/2, k^2)$, $\tau^2 = \tilde{\beta}\tilde{\alpha}$ where $IG(\cdot, \cdot)$, $G(\cdot, \cdot)$ are the Inverse Gamma and Gamma distributions and τ follows a half-Cauchy distribution with scale k . We re-express the whole SS-GHS prior hierarchy as:

$$\begin{aligned}\pi(\bar{\mathbf{w}}_{lj}|z_{lj}) &= (1 - z_{lj})\delta_0 + z_{lj}N(0, \sigma_0^2\tilde{\tau}_{lj}^2s^2\mathbf{I}), \tilde{\tau}_{lj}^2 = (c^2\beta_{lj}\alpha_{lj})(c^2 + \beta_{lj}\alpha_{lj}s_as_b)^{-1} \\ \pi(z_{lj}) &= \text{Ber}(\lambda_l) \\ \pi(\beta_{lj}) &= IG(1/2, 1), \pi(\alpha_{lj}) = G(1/2, 1), \pi(s_b) = IG(1/2, 1), \pi(s_a) = G(1/2, s_0^2)\end{aligned}\quad (11)$$

Variational family: We consider the following fully factorized variational family

$$\begin{aligned}q(\bar{\mathbf{w}}_{lj}|z_{lj}) &= (1 - z_{lj})\delta_0 + z_{lj}N(\boldsymbol{\mu}_{lj}, \text{diag}(\boldsymbol{\sigma}_{lj}^2)) \\ q(z_{lj}) &= \text{Ber}(\gamma_{lj}) \\ q(\beta_{lj}) &= LN(\mu_{lj}^{\{\beta\}}, \sigma_{lj}^{\{\beta\}^2}), q(\alpha_{lj}) = LN(\mu_{lj}^{\{\alpha\}}, \sigma_{lj}^{\{\alpha\}^2}) \\ q(s_b) &= LN(\mu^{\{s_b\}}, \sigma^{\{s_b\}^2}), q(s_a) = LN(\mu^{\{s_a\}}, \sigma^{\{s_a\}^2})\end{aligned}\quad (12)$$

for $l = 0, \dots, L$, $j = 1, \dots, k_{l+1}$. Similar to SS-GL variational family, we use the Log-Normal family instead of the Gamma and Inverse-Gamma families to approximate Gamma and Inverse-Gamma distributed variables to facilitate numerical optimization. Lastly, $(\mu_{lj}^{\{\beta\}}, \sigma_{lj}^{\{\beta\}^2})$, $(\mu_{lj}^{\{\alpha\}}, \sigma_{lj}^{\{\alpha\}^2})$, $(\mu^{\{s_b\}}, \sigma^{\{s_b\}^2})$, and $(\mu^{\{s_a\}}, \sigma^{\{s_a\}^2})$ are the variational mean and standard deviation parameters of the Gaussian distributions $q(\log \beta_{lj})$, $q(\log \alpha_{lj})$, $q(\log s_b)$ and $q(\log s_a)$.

ELBO: Let $\boldsymbol{\theta}$ be the network weights and $\boldsymbol{\omega} = (\mathbf{z}, \boldsymbol{\tau}^2, s^2)$ be the remaining parameters. We minimize the loss function $\mathcal{L} = -\text{ELBO}(q(\boldsymbol{\theta}, \boldsymbol{\omega}), \pi(\boldsymbol{\theta}, \boldsymbol{\omega}|\mathcal{D}))$ where

$$\begin{aligned}\mathcal{L} &= -\mathbb{E}_{q(\boldsymbol{\theta}, \boldsymbol{\omega})}[\log L(\boldsymbol{\theta})] + \sum_{l,i} d_{\text{KL}}(\text{Ber}(\gamma_{lj}), \text{Ber}(\lambda_l)) \\ &+ \int \int \left[\sum_{l,j} q(z_{lj} = 1) \int \int d_{\text{KL}}(N(\boldsymbol{\mu}_{lj}, \text{diag}(\boldsymbol{\sigma}_{lj}^2)), N(0, \sigma_0^2\tilde{\tau}_{lj}^2s^2\mathbf{I})) \right] dQ(\beta_{lj}, \alpha_{lj}, s_a, s_b) \\ &+ \sum_{l,j} \left[d_{\text{KL}}(LN(\mu_{lj}^{\{\beta\}}, \sigma_{lj}^{\{\beta\}^2}), IG(1/2, 1)) + d_{\text{KL}}(LN(\mu_{lj}^{\{\alpha\}}, \sigma_{lj}^{\{\alpha\}^2}), G(1/2, 1)) \right] \\ &+ d_{\text{KL}}(LN(\mu^{\{s_b\}}, \sigma^{\{s_b\}^2}), IG(1/2, 1)) + d_{\text{KL}}(LN(\mu^{\{s_a\}}, \sigma^{\{s_a\}^2}), G(1/2, s_0^2))\end{aligned}$$

where $dQ(\beta_{lj}, \alpha_{lj}, s_b, s_a) = q(\beta_{lj})q(\alpha_{lj})q(s_b)q(s_a)d\beta_{lj}d\alpha_{lj}ds_bds_a$.

3.3 Algorithm and Computational Details

We minimise the loss \mathcal{L} for both SS-GL and SS-GHS models by recursively sampling their corresponding variational posterior, allowing us to propagate the information through the network. The Gaussian variational approximations, $N(\boldsymbol{\mu}_{lj}, \text{diag}(\boldsymbol{\sigma}_{lj}^2))$, are reparameterized as $\boldsymbol{\mu}_{lj} + \boldsymbol{\sigma}_{lj} \odot \boldsymbol{\zeta}_{lj}$ for $\boldsymbol{\zeta}_{lj} \sim N(0, \mathbf{I})$, where \odot denotes the entry-wise (Hadamard) product.

Continuous Relaxation. The discrete spike variables (\mathbf{z}) are replaced with their continuous relaxation to circumvent the nondifferentiability in \mathcal{L} (Jang et al., 2017; Maddison et al., 2017). Specifically, the Gumbel-softmax (GS) distribution is used for continuous relaxation, that is $q(z_{lj}) \sim \text{Ber}(\gamma_{lj})$ is approximated by

$q(\tilde{z}_{lj}) \sim \text{GS}(\gamma_{lj}, \tau)$, where

$$\tilde{z}_{lj} = (1 + \exp(-\eta_{lj}/\tau))^{-1}, \quad \eta_{lj} = \log(\gamma_{lj}/(1 - \gamma_{lj})) + \log(u_{lj}/(1 - u_{lj})), \quad u_{lj} \sim U(0, 1)$$

where τ , the temperature parameter is chosen as 0.5 (Jantre et al., 2022). Using \tilde{z}_{lj} in backward pass eases gradient calculation. Using z_{lj} in forward pass gives exact node sparsity.

Algorithm 1 Variational inference in SS-GL and SS-GHS Bayesian neural networks

Inputs: training dataset, network architecture, and optimizer tuning parameters.

Model inputs: prior parameters for $\mathcal{T} = (\boldsymbol{\theta}, \mathbf{z}, \boldsymbol{\tau}^2)$ in SS-GL and $\mathcal{T} = (\boldsymbol{\theta}, \mathbf{z}, \boldsymbol{\tau}^2, s^2)$ in SS-GHS.

Variational inputs: number of Monte Carlo samples S .

Output: Variational parameter estimates of network weights, scales, and sparsity.

Method: Set initial values of variational parameters.

repeat

 Generate S samples of $\boldsymbol{\beta}_{lj}, z_{lj}, \tilde{z}_{lj}, \tau_{lj}^2, s^2$ (s^2 for SS-GHS)

 Use $\boldsymbol{\beta}_{lj}, \tau_{lj}^2, s^2$ and z_{lj} to compute \mathcal{L} in forward pass

 Use $\boldsymbol{\beta}_{lj}, \tau_{lj}^2, s^2$ and \tilde{z}_{lj} to compute gradient of \mathcal{L} in backward pass

 Update the variational parameters with gradient of loss using stochastic gradient descent algorithm (e.g. SGD with momentum (Sutskever et al., 2013))

until change in ELBO $< \epsilon$

4 Structurally Sparse BNNs: Theory

In this section, we prove the variational posterior consistency for both of our spike-and-slab models and also derive the posterior concentration rates. Let $\overline{\mathbf{W}}_l = (\mathbf{w}_{l1}^\top, \dots, \mathbf{w}_{lk_{l+1}}^\top)^\top$ and $\tilde{\mathbf{w}}_l = (\|\mathbf{w}_{l1}\|_2, \dots, \|\mathbf{w}_{lk_{l+1}}\|_2)$ be the vector of L_2 norms of rows of $\overline{\mathbf{W}}_l$. Our theoretical framework relies on three neural network architecture specific assumptions: (1) the number of nodes can vary with the layer index, i.e, $\mathbf{k} = (k_0, \dots, k_{L+1})$ is the node vector (2) the best sparse neural network approximation to the function η_0 may have varying number of nodes in each layer, hence, layer-wise node sparsity $\mathbf{s} = (s_1, \dots, s_L)$ (3) the best neural network approximation to η_0 may have varying bounds per layer, $\mathbf{B} = (B_1, \dots, B_L)$, on the L_2 norm of the incoming weights (including the bias term) onto the node for each layer.

Let f_0 and f_θ be the joint density of the observations $(y_i, \mathbf{x}_i)_{i=1}^n$ under the truth and the model respectively. For the theoretical developments, we assume $\mathbf{X} \sim U[0, 1]^p$, which implies $f_0(\mathbf{x}) = f_\theta(\mathbf{x}) = 1$ and the joint distribution of $(y_i, \mathbf{x}_i)_{i=1}^n$ depends only on conditional distribution of $Y|X = \mathbf{x}$, i.e, $P_0 = f_0(y|\mathbf{x})f_0(\mathbf{x}) = f_0(y|\mathbf{x})$ and similarly $P_\theta = f_\theta(y|\mathbf{x})$. This assumption on \mathbf{X} is quite common for posterior consistency (Polson and Ročková, 2018; Sun et al., 2021) and holds in bounded data (e.g. image datasets) through normalization.

We consider the following generalized sieve (see definition A.1 in Jantre et al. (2022)) $\mathcal{F}(L, \mathbf{k}, \mathbf{s}, \mathbf{B}) = \{\eta_\theta \in (2) : \|\tilde{\mathbf{w}}_l\|_0 \leq s_l, \|\tilde{\mathbf{w}}_l\|_\infty \leq B_l\}$. Let the L_2 distance between true function η_0 and all neural networks in $\mathcal{F}(L, \mathbf{k}, \mathbf{s}, \mathbf{B})$ by

$$\xi = \min_{\eta_\theta \in \mathcal{F}(L, \mathbf{k}, \mathbf{s}, \mathbf{B})} \|\eta_\theta - \eta_0\|_\infty^2. \quad (13)$$

Next, consider any sequence $\epsilon_n \rightarrow 0$. In the following two theorems, we establish the variational posterior consistency of $\tilde{\Pi}^*$, i.e the variational posterior concentrates in shrinking ϵ_n -Hellinger neighborhoods (Appendix A definition 6) of the true density P_0 with large probability. We denote the complement of the

Hellinger neighborhood of radius ϵ_n by

$$\mathcal{H}_{\epsilon_n}^c = \{\boldsymbol{\theta} : d_{\text{H}}(P_0, P_{\boldsymbol{\theta}}) > \epsilon_n\}.$$

Assume the following conditions:

- A.1 The activation function $\psi(\cdot)$ is 1-Lipschitz continuous upto a constant (e.g. relu, silu).
- A.2 The hyperparameter σ_0^2 is fixed at 1.
- A.3 The number of nodes in each layer k_l increase with increasing training data size.

4.1 Posterior Consistency for Group Lasso and Group Horseshoe

To provide the posterior contraction rate of the variational posterior for the Group Lasso, consider the prior and the variational family as in (8) and (9) respectively. Let

$$\begin{aligned} u_l &= \log n + \log L + \sum \log k_l + \sum \log(k_l + 1) - \log \min(1, \zeta^2) \\ \vartheta_l &= -\log\left(\frac{B_l^2}{(k_l + 1)}\left(\frac{\zeta^2}{k_l + 1}\right)\right) + \frac{B_l^2}{(k_l + 1)}\left(\frac{\zeta^2}{k_l + 1}\right) + 2 \log n + 2L + 2 \sum \log B_m \\ r_l &= s_l(k_l + 1)\vartheta_l/n \end{aligned} \tag{14}$$

Theorem 1. *Suppose A.1-A.3 hold. Let $\epsilon_n = \sqrt{(\sum_{l=0}^L r_l + \xi) \sum_{l=0}^L u_l}$ with r_l, u_l as in (14) and ξ as in (13). For a sequence $M_n \rightarrow \infty, M_n \epsilon_n \rightarrow 0$, the variational posterior $\tilde{\Pi}^*$ satisfies,*

$$\tilde{\Pi}^*(\mathcal{H}_{M_n \epsilon_n}^c) \xrightarrow{P_n^0} 0, \quad n \rightarrow \infty$$

The above theorem quantifies the rate of contraction of the variational posterior in the case of Group Lasso. Note that the two main quantities that control the rate are $B_l^2/(k_l + 1)$ and $\zeta^2/(k_l + 1)$. The quantity $B_l^2/(k_l + 1)$ indicates the effective strength of the weights incident onto a node and $\zeta^2/(k_l + 1)$ denotes the penalty imposed on the effective strength. Although lower values of $\zeta^2/(k_l + 1)$ give better contraction rates, too small values may cause $-\log(B_l^2 \zeta^2/(k_l + 1)^2)$ to explode. One must also guard against too small values of ζ^2 or else $-\log \min(1, \zeta^2)$ may not be $o(n \epsilon_n^2)$.

The following corollary gives the conditions on the hyperparameters σ_0^2 and λ_l to guarantee the convergence of the variational posterior for the Group Lasso.

Corollary 2. *Let $\sigma_0^2 = 1, \vartheta_l$ as in (14) and $-\log \lambda_l = \log(k_{l+1}) + C_l(k_l + 1)\vartheta_l$, then conditions of Theorem 1 hold.*

To provide the posterior contraction rate of the variational posterior for the Group Horseshoe, consider the half-Cauchy prior as in (10). Following Bai and Ghosh (2018) we can make the following regularity assumption on the half-Cauchy priors. Let $\pi(t)$ denote the density function of the random variable T .

- A.4 If $\sqrt{T} \sim C^+(0, 1)$, then $\pi(t) = K(t)^{-a-1}L(t)$ for some constant $a > 0$ and $L(t) \geq c_0$ for all $t \geq t_0$ and some constant $c_0 > 0$.
- A.5 If $\sqrt{T} \sim C^+(0, s_0)$, then $\pi(t) = K(t)^{-a'-1}L(t)$ for some constant $a' > 0$ and $L(t) \geq c'_0$ for all $t \geq t'_0$ and some constant $c'_0 > 0$.

We next define the following quantities

$$\begin{aligned}
u_l &= \log n + \log L + \sum \log k_l + \sum \log(k_l + 1) + \log c^2 \\
\vartheta_l &= -\log\left(\frac{B_l^2}{(k_l + 1)}\left(\frac{1}{t_0 t'_0} + \frac{1}{c^2}\right)\right) + \frac{B_l^2}{(k_l + 1)}\left(\frac{1}{t_0 t'_0} + \frac{1}{c^2}\right) + 2\log n + 2L + 2\sum \log B_m \\
r_l &= s_l(k_l + 1)\vartheta_l/n
\end{aligned} \tag{15}$$

For the prior formulation and variational family as in (11) and (12) respectively, we have

Theorem 3. *Let A.1-A.5 hold. Let $\epsilon_n = \sqrt{(\sum_{l=0}^L r_l + \xi) \sum_{l=0}^L u_l}$ with r_l, u_l as in (15) and ξ as in (13). For a sequence $M_n \rightarrow \infty, M_n \epsilon_n \rightarrow 0$, the variational posterior $\tilde{\Pi}^*$ satisfies,*

$$\tilde{\Pi}^*(\mathcal{H}_{M_n \epsilon_n}^c) \xrightarrow{P_n^0} 0, \quad n \rightarrow \infty$$

The above theorem quantifies the rate of contraction of the variational posterior in the case of Group Horseshoe. Note that the two main quantities that control the rate are $B_l^2/(k_l + 1)$ and $(1/t_0 t'_0 + 1/c^2)$. The quantity $B_l^2/(k_l + 1)$ indicates the effective strength of the weights incident onto a node and $(1/t_0 t'_0 + 1/c^2)$ denotes the penalty imposed on the effective strength. Although lower values of $(1/t_0 t'_0 + 1/c^2)$ lead to better shrinkage, too small values may cause $-\log(B_l(1/t_0 t'_0 + 1/c^2)/(k_l + 1))$ to explode. One must also guard against too large values of $\log c^2$ or else $\log c^2$ may not be $o(n\epsilon_n^2)$.

The following corollary gives the conditions on the hyperparameters $\sigma_0^2 = 1$ and λ_l to guarantee the convergence of the variational posterior for the Group Horseshoe.

Corollary 4. *Let $\sigma_0^2 = 1, \vartheta_l$ as in (15) and $-\log \lambda_l = \log(k_{l+1}) + C_l(k_l + 1)\vartheta_l$, then conditions of Theorem 3 hold.*

The contraction rates of both Group Lasso and Group Horseshoe depend mainly on r_l and ξ . Note, r_l controls the number of nodes in the neural network. If the network is not sparse, then r_l is $k_{l+1}(k_l + 1)\vartheta_l/n$ instead of $s_l(k_l + 1)\vartheta_l/n$. This will make the convergence of $\epsilon_n \rightarrow 0$ difficult. If s_l and $B_l^2/(k_l + 1)$ are too small, it will cause ξ to explode since a good approximation to the true function may not exist in a very sparse space.

Remark 5. *Consider the generic form $\vartheta_l = -\log(\lambda^* B_l^2/(k_l + 1)) + \lambda^* B_l^2/(k_l + 1) + 2\log n + 2L + 2\sum \log B_m$ where λ^* behaves like a penalization constant. For a simple spike-and-slab Gaussian prior and spike-and-slab mean field Gaussian variational family, the variational posterior contraction holds with $\lambda^* = 1$. As in Theorems 1 and 3, the penalization constant λ^* is $\zeta^2/(k_l + 1)$ and $(1/t_0 t'_0 + 1/c^2)$ for Group Lasso and Group Horseshoe respectively. Note, if for a nonparametric function, the best approximating neural network has exploding values of $B_l^2/(k_l + 1)$, Group Lasso with $\zeta^2 < k_l + 1$ and $c^2 \rightarrow \infty$ may produce better contraction rates than Gaussian. On the other hand, if the best approximating neural network has shrinking values of $B_l^2/(k_l + 1)$, Group Horseshoe with $c = 1$ and Group Lasso with $\zeta^2 > k_l + 1$ is expected to produce better contraction rates than Gaussian.*

5 Experiments

In this section, we demonstrate the performance of our proposed **SS-GL** and **SS-GHS** approaches on network architectures and techniques used in practice. We consider multilayer perceptron (MLP), LeNet-5-Caffe, and ResNet architectures which we implement in PyTorch (Paszke et al., 2019). We perform image

classification using the aforementioned neural networks in widely used MNIST, Fashion-MNIST, and CIFAR-10 datasets.

In all the experiments, we fix $\sigma_0^2 = 1$ and $\sigma_\epsilon^2 = 1$. The remaining tuning parameter details such as learning rate, minibatch size, and initial parameter choice are provided in the appendix E. The prediction accuracy is calculated using a variational Bayes posterior mean estimator with 10 Monte Carlo samples at test time. We use swish (SiLU) activations (Elfwing et al., 2018; Ramachandran et al., 2017) instead of ReLU for our proposed SS-GL and SS-GHS models and for Jantre et al. (2022)’s spike-and-slab Gaussian node selection model (SS-IG) to avoid the dying neuron problem (Lu et al., 2020). Other smoother activation functions could be used but swish displayed the best performance.

We provide node sparsity estimates for each linear hidden layer separately. For all models, the node sparsity in a given linear layer is the ratio of the number of neurons with at least one nonzero incoming edge over the original number of neurons present in that layer before training. In a convolution layer, we provide channel sparsity estimate which is the ratio of the number of output channels with at least one nonzero incoming connection over the total number of output channels present in the dense counterpart. The layer-wise node or channel sparsity estimates provide a granular illustration of the structural compactness of the trained model. The structural sparsity in the trained model leads to lower computational complexity at test time which is vital for resource-constrained devices.

5.1 MLP MNIST Classification

In this experiment, we use MLP model with 2 hidden layers having 400 nodes per layer to fit the MNIST data which consists of 60,000 small square 28×28 pixel grayscale images of handwritten single digits between 0 and 9. We preprocess the images in the MNIST data by dividing their pixel values by 126. The output layer has 10 neurons since there are 10 classes in the MNIST data. We provide the graph of the prediction accuracy of the i.i.d. test data over a training period of 1200 epochs. We provide layer-wise node sparsity plots for both layers to highlight the dynamic structural compactness of the model under training. In what follows, we discuss the choice of ζ^2 in (8) for the SS-GL model and the c values (referred to as c_{reg} in this section) in (10) for the SS-GHS model.

SS-GL penalty parameter choice. In Theorem 1, we have derived the variational posterior consistency in SS-GL model under the assumption that ζ^2 is constant. However, the value of ζ^2 needs to be carefully tuned for numerical experiments (Xu and Ghosh, 2015). A very large value of ζ^2 will overshrink the network weights and lead to biased estimates; $\zeta^2 \rightarrow 0$ will lead to a very diffuse distribution for the slab part. Instead, we place a conjugate Gamma prior on the penalty parameter, $\zeta^2 \sim \Gamma(c, d)$, and estimate it through our variational inference framework via an approximating family $q(\zeta^2) := LN(\mu_\zeta, \sigma_\zeta^2)$.

Figure 2 summarizes the results of the MLP-MNIST experiment using SS-GL model with fixed $\zeta^2 = 1$ and variable $\zeta^2 \sim \Gamma(c = 4, d = 2)$. The values of the shape ($c = 4$) and rate ($d = 2$) parameters were chosen based on hyperparameter search and past literature. We observe that inferring the value of ζ^2 from Bayesian estimation significantly improves the predictive accuracy compared to fixed ζ^2 (Figure 2a). The fixed ζ^2 model has better node sparsities in both the layers of the MLP model (Figure 2b and 2c). This suggests that $\zeta^2 = 1$ might be overshrinking the weights which assist in pruning them via spike-and-slab prior, however, this also hampers the predictive performance of the model. In rest of the experiments involving SS-GL, we place the gamma prior on $\zeta^2 \sim \Gamma(c = 4, d = 2)$.

SS-GHS regularization constant choice. In Corollary 4, we provide the contraction rates for variational posterior in SS-GHS model for the regularization constant c_{reg} . Here we experiment with two values of the constant $c_{\text{reg}} = 1$ and $c_{\text{reg}} = k_l + 1$. The choice of $c_{\text{reg}} = 1$ makes the Horseshoe tails closer to Gaussian whereas $c_{\text{reg}} = k_l + 1$ makes it closer to the unregularized Horseshoe. Here, we provide an MLP-MNIST

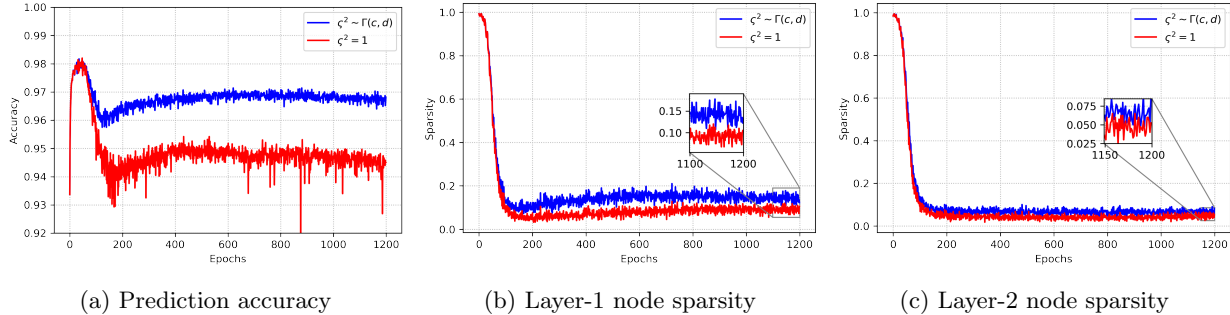


Figure 2: **SS-GL ζ^2 choice experiment.** Here, we demonstrate the performance of our SS-GL with fixed $\zeta^2 = 1$ and variable $\zeta^2 \sim \Gamma(c = 4, d = 2)$. (a) we plot the classification accuracy on the test data. (b) and (c) we plot the proportion of active nodes (node sparsity) in layer-1 and layer-2 of the network respectively. We observe that placing a prior on ζ^2 yields better classification accuracy.

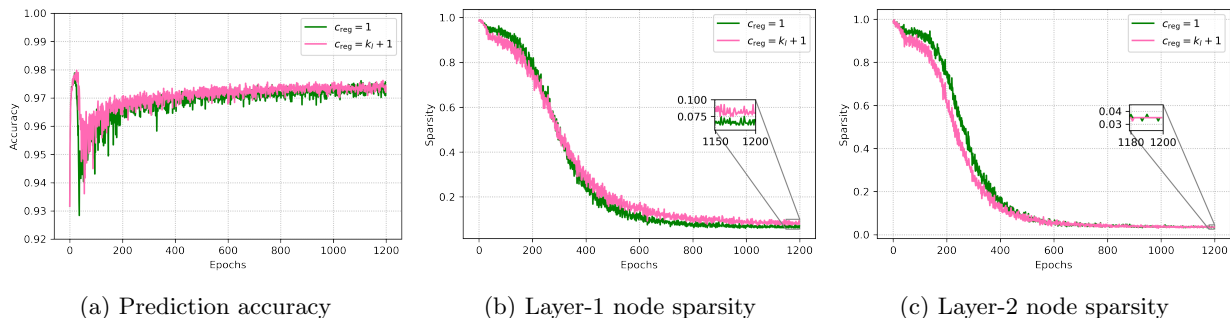


Figure 3: **SS-GHS c_{reg} choice experiment.** Here, we demonstrate the performance of our SS-GHS with regularization constant of $c_{\text{reg}} = 1$ and $c_{\text{reg}} = k_l + 1 = 401$. (a) we plot the classification accuracy on the test data. (b) and (c) we plot the proportion of active nodes (node sparsity) in layer-1 and layer-2 of the network respectively. We observe that both c_{reg} choices lead to similar classification accuracies with $c_{\text{reg}} = 1$ having better layer-1 node sparsity.

experiment using SS-GHS model with aforementioned c_{reg} values. In MLP, the $k_l + 1 = 400 + 1 = 401$ is a large constant and essentially acts as an unregularized model. We ran an unregularized version of the model and verified this claim but do not provide the results for brevity.

Figure 3 summarizes the results of MLP-MNIST experiment using SS-GHS model $c_{\text{reg}} = 1$ and $c_{\text{reg}} = k_l + 1$. We observe that both values of c_{reg} lead to same predictive accuracies on test data. However in $c_{\text{reg}} = 1$ scenario, SS-GHS model has better layer-1 node sparsity (Figure 3b). Layer-2 node sparsity is same in both the c_{reg} values (Figure 3c). In rest of the experiments involving SS-GHS, we choose $c_{\text{reg}} = 1$.

MLP-MNIST comparison with SS-IG

We provide an MLP-MNIST experiment where we compare our proposed models with the SS-IG model. The results are presented in Figure 4. We provide test data accuracy, model compression ratio, flops ratio, and layer-wise node sparsities in each experiment.

Additional metrics. We provide two additional metrics that relate to the model compression and computational complexity. (i) *compression ratio*: it is the ratio of the number of nonzero weights in the compressed network versus the dense model and is an indicator of storage cost at test-time. (ii) *floating point operations (FLOPs) ratio*: it is the ratio of the number of FLOPs required to predict the output from the input during

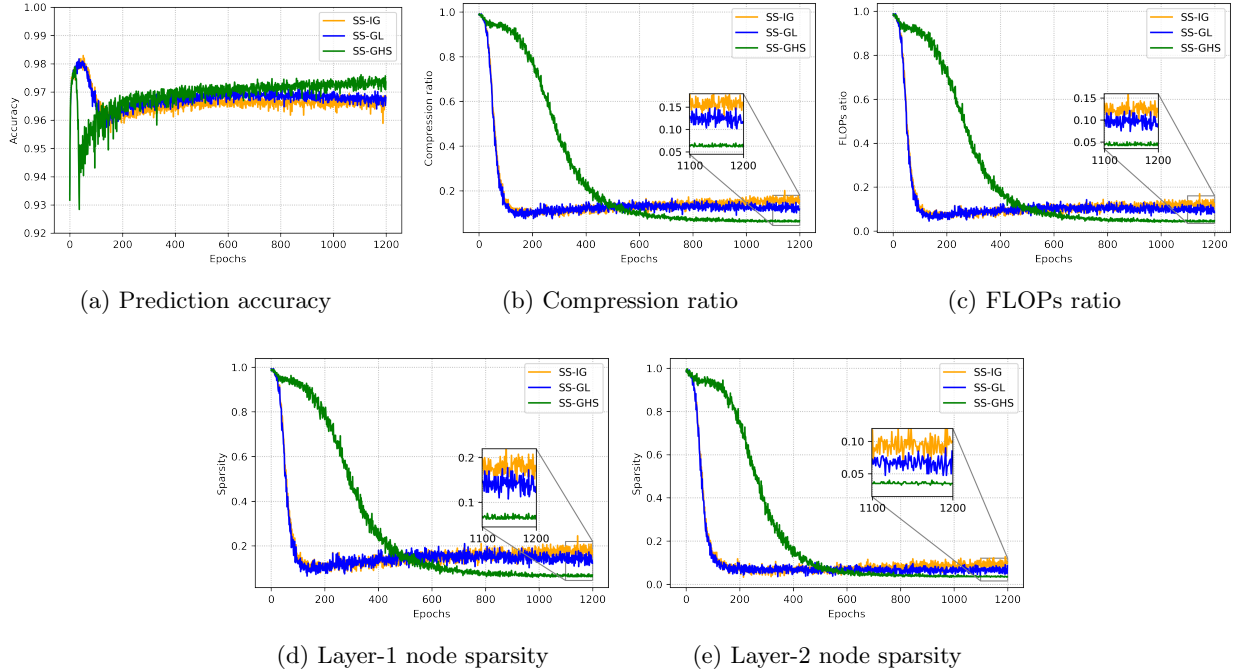


Figure 4: **Main MLP-MNIST experiment.** Here, we demonstrate the performance of our SS-GL ($\zeta^2 \sim \Gamma(c = 4, d = 2)$) and SS-GHS ($c_{\text{reg}} = 1$) models compared against SS-IG model. (a) we plot the classification accuracy on the test data. (b) and (c) we plot the proportion of active nodes (node sparsity) in layer-1 and layer-2 of the network respectively. We observe that our SS-GHS yields the most compact network with the best classification accuracy.

test-time in the compressed network versus its dense counterpart. We have detailed the FLOPs calculation in neural networks in Appendix E. Layer-wise node and channel sparsities are directly related to the FLOPs ratio and we only provide the FLOPs ratio in LeNet-5-Caffe and ResNet models for brevity.

In Figure 4a, we observe that SS-GHS has better predictive accuracy compared to SS-GL and SS-IG models. Moreover, the SS-GHS model not only has minimal storage cost among the node selection models compared (Figure 4b) but also the least number of FLOPs required for inference during test-time (Figure 4c). In Figure 4d and 4e, we observe that SS-GHS has pruned away a maximum number of nodes in contrast to SS-GL and SS-IG models and this also leads to the maximum reduction in FLOPs evident from (Figure 4c). Lastly, SS-GL and SS-IG models have similar predictive accuracies; however, SS-GL has lower layer-wise node sparsities in both layers, hence the lower FLOPs ratio and it also has lower storage cost at test-time compared to SS-IG.

5.2 LeNet-5-Caffe Experiments

The results of more complex LeNet-5-Caffe network experiments on MNIST and Fashion-MNIST are presented in Figure 5. We provide test data accuracy, model compression ratio, and FLOPs ratio in each experiment over 1200 epochs. Here, the FLOPs ratio serves as a collective indicator of layer-wise node sparsities since FLOPs are directly related to how many neurons or channels are remaining in linear or convolution layers respectively.

In LeNet-5-Caffe-MNIST experiment (Figure 5a - 5c), we observe that our SS-GHS and SS-GL models have better predictive accuracy than SS-IG (Figure 5a). We observe that both SS-GHS and SS-GL models

have better model compression ratios (Figure 5b). Moreover, all three models compared achieve a similar reduction in Flops (Figure 5c). In contrast with the MLP-MNIST experiment (Figure 4) our SS-GHS and SS-GL have the same performance on all metrics in the LeNet-5-Caffe-MNIST experiment.

In LeNet-5-Caffe-Fashion-MNIST experiment (Figure 5d - 5f), we observe that SS-GHS has better predictive accuracy compared to SS-GL and SS-IG models. The storage cost reduction in the SS-GHS model is similar to SS-IG but better than SS-GL (Figure 5e). Next, SS-IG achieves the best reduction in FLOPs compared to both our approaches and SS-GHS has lower FLOPs than SS-GL. Lastly, SS-GL and SS-IG models have similar predictive accuracies; however, SS-IG has lower FLOPs and storage cost at test time.

5.3 Residual Network Experiments

This section presents an example demonstrating the trade-off between the computational complexity and memory cost at test-time among our structured pruning methods and recent unstructured pruning methods in Residual Networks (ResNet) applied on CIFAR-10 dataset (He et al., 2016). The dataset consists of 60000 32x32 color images in 10 classes. There are 50000 training images and 10000 test images. We use ResNet-20 and ResNet-32 architectures and follow the experimental setting provided by Sun et al. (2021). We compare our proposed SS-GL and SS-GHS methods with SS-IG (Jantre et al., 2022), consistent sparse deep learning (BNN_{cs}) (Sun et al., 2021), and variational Bayes neural network with mixture Gaussian prior (VBNN) (Blundell et al., 2015). In all of our experiments, we follow the same training setup as used in Sun et al. (2021) and Zhong et al. (2020).

In all the models, we set $\sigma_e^2 = 1$ and $\sigma_0^2 = 0.04$ same as Sun et al. (2021). In SS-IG, SS-GL, and SS-GHS we use common $\lambda_l = 10^{-4}$ after hyperparameter search since our theory does not cover Bayesian CNNs. However, posterior consistency in Bayesian CNNs is an interesting future direction of work.

We quantify the predictive performance using the accuracy of the test data. Besides the test accuracy,

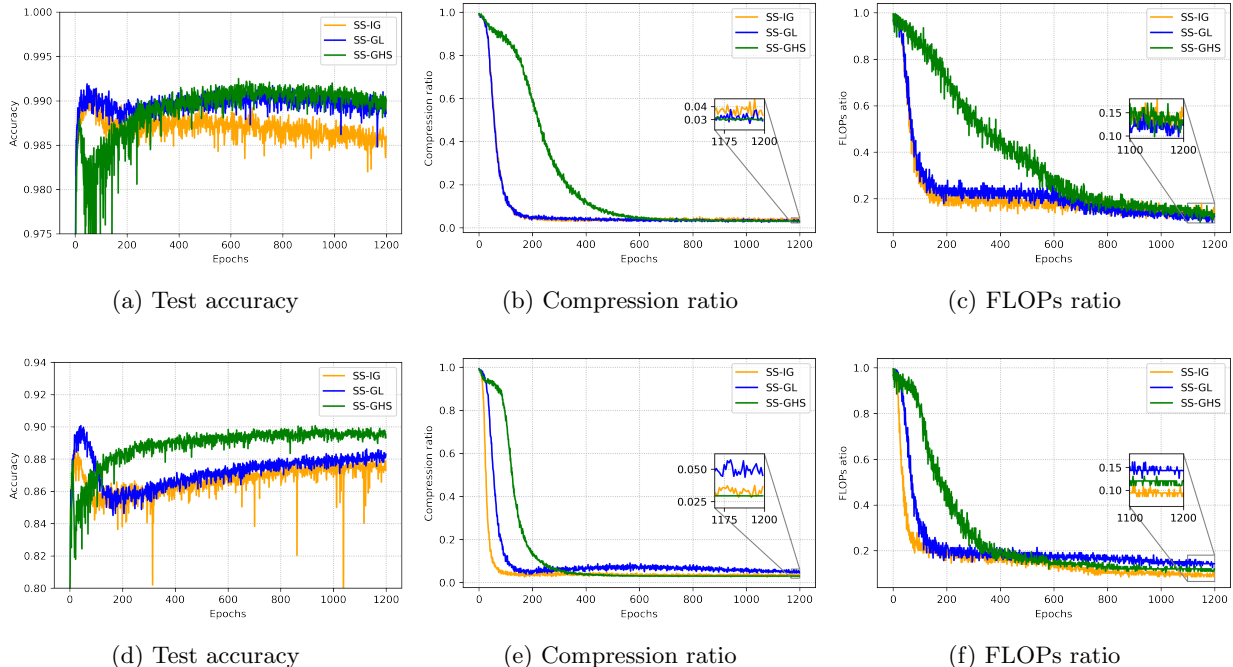


Figure 5: LeNet-5-Caffe network experiment results. Top row (a)-(c) represent the LeNet-5-Caffe on MNIST experiment results. Bottom row (d)-(f) represent the LeNet-5-Caffe on Fashion-MNIST experiment results.

Table 1: ResNet-CIFAR-10 experiment results. The results of each method is calculated by averaging over 3 independent runs with standard deviation reported in parentheses. For BNN_{cs} and VBNN models, we show predefined percentages of pruned parameters used for magnitude pruning given in (Sun et al., 2021).

Model	Method	Test Accuracy	Compression (%)	Pruned FLOPs (%)
ResNet-20	BNN_{cs} (20%)	92.23 (0.16)	19.29 (0.12)	98.94 (0.38)
	BNN_{cs} (10%)	91.43 (0.11)	9.18 (0.13)	99.13 (0.37)
	VBNN (20%)	89.61 (0.04)	19.55 (0.01)	100.00 (0.00)
	VBNN (10%)	88.43 (0.13)	9.50 (0.00)	99.93 (0.00)
	SS-IG	92.94 (0.15)	79.52 (0.98)	88.39 (1.00)
	SS-GL (ours)	92.99 (0.11)	76.10 (1.55)	85.15 (1.76)
	SS-GHS (ours)	92.87 (0.23)	78.70 (0.42)	86.18 (1.02)
ResNet-32	BNN_{cs} (10%)	92.65 (0.03)	9.15 (0.03)	94.53 (0.86)
	BNN_{cs} (5%)	91.39 (0.08)	4.49 (0.02)	90.79 (1.35)
	VBNN (10%)	89.37 (0.04)	9.61 (0.01)	99.99 (0.02)
	VBNN (5%)	87.38 (0.22)	4.59 (0.01)	94.27 (0.54)
	SS-IG	93.08 (0.23)	55.28 (2.96)	67.59 (2.36)
	SS-GL (ours)	93.33 (0.11)	54.27 (1.73)	66.93 (2.98)
	SS-GHS (ours)	93.15 (0.23)	53.72 (2.11)	66.68 (2.75)

we use *compression (%)* and *pruned FLOPs (%)* which are compression ratio and FLOPs ratio discussed earlier converted to percentages respectively. In this experiment, we only count parameters and FLOPs over the convolutional and last fully connected layer, because our proposed methods focus on channel and node pruning of convolutional and linear layers respectively.

For ResNet architecture, our proposed methods under centered parameterization similar to previous experiments in Section 5.1 and 5.2 have unstable performance. Instead, we incorporate non-centered parameterization (Ghosh et al., 2019) to stabilize the training. Below we detail the non-centered parameterization strategy:

Non-Centered Parameterization: We adopt non-centered parameterization for the slab component in both the prior setups to circumvent the pathological funnel-shaped geometries associated with the coupled posterior (Ingraham and Marks, 2017; Ghosh et al., 2019). Let $\tau_{l_j}^{*2} = \tau_{l_j}^2$ (for SS-GL) or $\tau_{l_j}^{*2} = \tilde{\tau}_{l_j}^2 s^2$ (for SS-GHS) leads to the following reparameterization of the priors in (8) and (11)

$$\pi(\bar{\mathbf{w}}_{l_j} | z_{l_j}) = (1 - z_{l_j})\delta_0 + z_{l_j}\tau_{l_j}^* \bar{\mathbf{w}}_{l_j}^{(0)}, \quad \pi(\bar{\mathbf{w}}_{l_j}^{(0)}) = N(0, \sigma_0^2 \mathbf{I})$$

Similarly, the variational families in (9) and (12) are reparameterized as

$$q(\bar{\mathbf{w}}_{l_j} | z_{l_j}) = (1 - z_{l_j})\delta_0 + z_{l_j}\tau_{l_j}^* \bar{\mathbf{w}}_{l_j}^{(0)}, \quad q(\bar{\mathbf{w}}_{l_j}^{(0)}) = N(\boldsymbol{\mu}_{l_j}, \text{diag}(\boldsymbol{\sigma}_{l_j}^2))$$

This formulation leads to simpler posterior geometries (Betancourt and Girolami, 2015). This non-centered reparameterization leads to efficient posterior inference without change in form of the prior but with a minor change in the form of the variational family.

We summarize the ResNet experiment results in Table 1. The comparison with BNN_{cs} and VBNN models indicates that our SS-GL and SS-GHS methods have significantly better prediction accuracy in both ResNet-20 and ResNet-32 setups. Moreover, we demonstrate that even though BNN_{cs} and VBNN models have predefined high levels of pruned parameters, our models have significantly fewer FLOPs during inference at test time. This highlights the trade-off between unstructured sparsity and structured sparsity

methods, where the former leads to a significant reduction in storage cost and the latter has significantly less computational complexity at test-time. In comparison with the SS-IG node selection model, we observe that our SS-GL and SS-GHS models have lower storage cost and FLOPS at test time with comparable predictive accuracy in ResNet-20 architecture. In ResNet-32 case, SS-GL has better predictive accuracy than SS-IG, while compression (%) and pruned FLOPs (%) in our models are comparable to SS-IG within standard deviation. This comparison further highlights the advantage of using group shrinkage priors instead of Gaussian in the slab part of the spike-and-slab framework to achieve better test accuracies with lower computational and memory footprint.

6 Conclusion

In this paper, we have used spike and Group shrinkage slab distributions to facilitate optimal node recovery. The two group shrinkage priors explored in this context include Group Lasso and Group Horseshoe. Our theoretical developments compare and contrast the variational posterior contraction rates for the two popular shrinkage priors. We also discuss the theoretical comparison of group shrinkage priors with that of a simple Gaussian prior. As a final contribution, in the context of node selection, we demonstrate the numerical efficacy of using spike-and-slab distributions with Group Lasso and Group Horseshoe as the choice for slab distributions. In particular, for a wide range of experiments including Lenet-Caffe and Residual Networks, we demonstrate that the node selection approach using group shrinkage priors leads to the smallest FLOPs ratio among all baseline approaches.

A Definitions and General Lemmas

A.1 Definitions

Definition 6. Hellinger neighborhood: We define the ε -Hellinger neighborhood of the true density P_0 with $\mathcal{H}_\varepsilon = \{\boldsymbol{\theta} : d_{\text{H}}(P_0, P_{\boldsymbol{\theta}}) < \varepsilon\}$ where the Hellinger distance, $d_{\text{H}}(P_0, P_{\boldsymbol{\theta}})$, between P_0 and the model density function $P_{\boldsymbol{\theta}}$ is given by

$$2d_{\text{H}}^2(P_0, P_{\boldsymbol{\theta}}) = \int_{\mathbf{x} \in [0,1]^p} \int \left(\sqrt{f_{\boldsymbol{\theta}}(y|\mathbf{x})} - \sqrt{f_0(y|\mathbf{x})} \right)^2 dy d\mathbf{x}$$

Definition 7. Kullback-Leibler neighborhood: The ε -KL neighborhood of P_0 is defined as $\mathcal{N}_\varepsilon = \{\boldsymbol{\theta} : d_{\text{KL}}(P_0, P_{\boldsymbol{\theta}}) < \varepsilon\}$ where the KL distance, $d_{\text{KL}}(P_0, P_{\boldsymbol{\theta}})$, between P_0 and $P_{\boldsymbol{\theta}}$ is

$$d_{\text{KL}}(P_0, P_{\boldsymbol{\theta}}) = \int_{\mathbf{x} \in [0,1]^p} \int \log \frac{f_0(y|\mathbf{x})}{f_{\boldsymbol{\theta}}(y|\mathbf{x})} f_0(y|\mathbf{x}) dy d\mathbf{x}$$

A.2 General Lemmas

Lemma 8. For any 1-Lipschitz continuous (with respect to absolute value) activation function ψ such that $|\psi(x)| \leq |x|$, $\forall x \in \mathbb{R}$,

$$N(\delta, \mathcal{F}(L, \mathbf{k}, \mathbf{s}, \mathbf{B}), \|\cdot\|_\infty) \leq \sum_{s_L^* \leq s_L} \cdots \sum_{s_0^* \leq s_0} \left[\prod_{l=0}^L \left(\frac{B_l}{\delta B_l / (2(L+1)(\prod_{j=0}^L B_j))} k_{l+1} \right)^{s_l} \right] \quad (16)$$

where N denotes the covering number.

Proof Refer to Lemma A.6 in Jantre et al. (2022). ■

B Requisite Lemmas for Theorems 1 and 3

Lemma 9 (Existence of Test Functions). *Let $\epsilon_n \rightarrow 0$ and $n\epsilon_n^2 \rightarrow \infty$. There exists a testing function $\phi \in [0, 1]$ and constants $C_1, C_2 > 0$,*

$$\begin{aligned} \mathbb{E}_{P_0}(\phi) &\leq \exp\{-C_1 n\epsilon_n^2\} \\ \sup_{\theta \in \mathcal{H}_{\epsilon_n}^c, \eta_{\theta} \in \mathcal{F}(L, \mathbf{k}, \mathbf{s}^\circ, \mathbf{B}^\circ)} \mathbb{E}_{P_\theta}(1 - \phi) &\leq \exp\{-C_2 n d_{\mathbb{H}}^2(P_0, P_\theta)\} \end{aligned}$$

where $\mathcal{H}_{\epsilon_n} = \{\theta : d_{\mathbb{H}}(P_0, P_\theta) \leq \epsilon_n\}$ is the Hellinger neighborhood of radius ϵ_n .

Proof Let $H = N(\epsilon_n/19, \mathcal{F}(L, \mathbf{k}, \mathbf{s}^\circ, \mathbf{B}^\circ), d_{\mathbb{H}}(\cdot, \cdot))$ denote the covering number of the $\mathcal{F}(L, \mathbf{k}, \mathbf{s}^\circ, \mathbf{B}^\circ)$. Using Lemma 8 with $\mathbf{s} = \mathbf{s}^\circ$ and $\mathbf{B} = \mathbf{B}^\circ$, we get

$$\begin{aligned} \log H &= \log N(\epsilon_n/19, \mathcal{F}(L, \mathbf{k}, \mathbf{s}^\circ, \mathbf{B}^\circ), d_{\mathbb{H}}(\cdot, \cdot)) \leq \log N(\sqrt{8}\sigma_e^2\epsilon_n/19, \mathcal{F}(L, \mathbf{k}, \mathbf{s}^\circ, \mathbf{B}^\circ), \|\cdot\|_\infty) \\ &\leq \log \left[\prod_{l=0}^L \left(\frac{38}{\sqrt{8}\sigma_e^2\epsilon_n} (L+1) \prod_{j=0}^L B_j^\circ k_{l+1} \right)^{(s_l^\circ+1)} \right] \\ &\leq C \left[\sum_{l=0}^L (s_l^\circ+1)(-\log \epsilon_n + \log(L+1)) + \sum_{j=0}^L \log B_j^\circ + \log k_{l+1} \right] \\ &\leq C \sum_{l=0}^L (s_l^\circ+1)(\log n + \log(L+1)) + \sum_{j=0}^L \log B_j^\circ + \log k_{l+1} \\ &\leq C \sum_{l=0}^L (s_l^\circ+1)(\log n + \log(L+1)) + \sum_{l=0}^L \log k_{l+1} + \sum_{l=0}^L \log(k_l+1) + A \leq Cn\epsilon_n^2 \end{aligned} \quad (17)$$

Group Lasso Case: $A = -\log \min(1, \varsigma^2)$. Next, let $B_l^\circ = 2(n\epsilon_n^2 + \log(k_l+1) + \log k_{l+1} + \log(L+1) + \log 4)(k_l+1)/\min(1, \varsigma^2)$ and $s_l^\circ+1 = n\epsilon_n^2/\sum_{l=0}^L u_l$ where $u_l = \log n + \log(L+1) + \sum_{l=0}^L \log k_l + \sum_{l=0}^L \log(k_l+1) - \log \min(1, \varsigma^2)$.

Group Horseshoe Case: $A = \log c^2$. Next, let $(B_l^\circ)^2 = 2(n\epsilon_n^2 + \log(k_l+1) + \log k_{l+1} + \log(L+1) + \log 2)(k_l+1)^2 c^2$ and $s_l^\circ+1 = n\epsilon_n^2/\sum_{l=0}^L u_l$ where $u_l = \log n + \log(L+1) + \sum_{l=0}^L \log k_l + \sum_{l=0}^L \log(k_l+1) + \log c^2$.

The remaining steps are the same as the Proof of Lemma 4.1 in Jantre et al. (2022). ■

Lemma 10 (Prior mass condition). *Let $\epsilon_n \rightarrow 0$, $n\epsilon_n^2 \rightarrow \infty$ and $n\epsilon_n^2/\sum_{l=0}^L u_l \rightarrow \infty$, then for prior $\tilde{\Pi}$ and some constant $C_3 > 0$, $\tilde{\Pi}(\mathcal{F}(L, \mathbf{k}, \mathbf{s}^\circ, \mathbf{B}^\circ)^c) \leq \exp(-C_3 n\epsilon_n^2/\sum_{l=0}^L u_l)$.*

Proof We provide proof for SS-GL in Appendix C and SS-GHS in Appendix D. ■

Lemma 11 has two conditions. Condition 1 requires that shrinking KL neighborhoods of the true density function P_0 get a sufficiently large probability to guarantee convergence of the true posterior in (5). Condition 2. helps control the KL distance between true posterior and variational posterior to guarantee the convergence of the variational posterior in (6).

Lemma 11 (Kullback-Leibler conditions). *Suppose $\sum_{l=0}^L r_l + \xi \rightarrow 0$ and $n(\sum_{l=0}^L r_l + \xi) \rightarrow \infty$. Assume the following two conditions hold for the prior $\tilde{\Pi}$ and some $q \in \mathcal{Q}$: (1) $\tilde{\Pi} \left(\mathcal{N}_{\sum_{l=0}^L r_l + \xi} \right) \geq \exp(-C_4 n(\sum_{l=0}^L r_l + \xi))$,*

(2) $d_{\text{KL}}(q, \pi) + n \sum_{\mathbf{z}} \int d_{\text{KL}}(P_0, P_{\boldsymbol{\theta}}) q(\boldsymbol{\theta}, \mathbf{z}) d\boldsymbol{\theta} \leq C_5 n (\sum_{l=0}^L r_l + \xi)$ where $\mathcal{N}_{\sum_{l=0}^L r_l + \xi}$ be the KL neighborhood of radius $\sum_{l=0}^L r_l + \xi$.

Proof The proof of this lemma differs in SS-GL and SS-GHS. We provide proof for the SS-GL in Appendix C and SS-GHS in Appendix D. ■

Lemma 12. *If Lemma 9 and Lemma 10 hold, then $\log \int_{\mathcal{H}_{\epsilon_n}^c} (P_{\boldsymbol{\theta}}^n / P_0^n) \pi(\boldsymbol{\theta}) d\boldsymbol{\theta} \leq -C n \epsilon_n^2 / \sum u_l$ with dominating probability.*

Proof Refer to Lemma A.8 in Jantre et al. (2022). ■

Lemma 13. *If Lemma 11 part 1 holds, for any $M_n \rightarrow \infty$, with dominating probability, $\log \int (P_0^n / P_{\boldsymbol{\theta}}^n) \tilde{\pi}(\boldsymbol{\theta}) d\boldsymbol{\theta} \leq n M_n (\sum r_l + \xi)$.*

Proof Refer to Lemma A.9 in Jantre et al. (2022). ■

Lemma 14. *If Lemma 11 part 2 holds, for any $M_n \rightarrow \infty$, with dominating probability, $d_{\text{KL}}(q, \pi) + \sum_{\mathbf{z}} \int \log(P_0^n / P_{\boldsymbol{\theta}}^n) q(\boldsymbol{\theta}, \mathbf{z}) d\boldsymbol{\theta} \leq n M_n (\sum r_l + \xi)$.*

Proof Refer to Lemma A.10 in Jantre et al. (2022). ■

C Spike-and-Slab Group Lasso Proofs

Proof of Lemma 10.

$$\text{Assumption : } s_l^\circ + 1 = (n \epsilon_n^2) / (\sum u_l), \quad \lambda_l k_{l+1} / s_l^\circ \rightarrow 0, \quad \sum u_l \log L = o(n \epsilon_n^2) \quad (18)$$

$$\begin{aligned} \tilde{\Pi}(\mathcal{F}(L, \mathbf{k}, \mathbf{s}^\circ, \mathbf{B}^\circ)^c) &\leq \tilde{\Pi} \left(\bigcup_{l=0}^L \{ \|\tilde{\mathbf{w}}_l\|_0 > s_l^\circ \} \right) + \tilde{\Pi} \left(\bigcup_{l=0}^L \{ \|\tilde{\mathbf{w}}_l\|_\infty > B_l^\circ \} \right) \\ &\leq \sum_{l=0}^L \tilde{\Pi}(\|\tilde{\mathbf{w}}_l\|_0 > s_l^\circ) + \sum_{l=0}^L \tilde{\Pi}(\|\tilde{\mathbf{w}}_l\|_\infty > B_l^\circ) \\ &= \sum_{l=0}^L \int \int \sum_{\mathbf{z}} \Pi(\|\tilde{\mathbf{w}}_l\|_0 > s_l^\circ | \boldsymbol{\tau}^2, \mathbf{z}) \pi(\mathbf{z}) \pi(\boldsymbol{\tau}^2) d\boldsymbol{\tau}^2 \\ &\quad + \sum_{l=0}^L \int \int \sum_{\mathbf{z}} \Pi(\|\tilde{\mathbf{w}}_l\|_\infty > B_l^\circ | \boldsymbol{\tau}^2, \mathbf{z}) \pi(\mathbf{z}) \pi(\boldsymbol{\tau}^2) d\boldsymbol{\tau}^2 \\ &\leq \sum_{l=0}^L \mathbb{P}(\sum_{i=1}^{k_{l+1}} z_{li} > s_l^\circ) + \sum_{l=0}^L \int \int \mathbb{P}(\sup_{i=1, \dots, k_{l+1}} \|\bar{\mathbf{w}}_{li}\|_2 > B_l^\circ | \boldsymbol{\tau}^2) \pi(\boldsymbol{\tau}^2) d\boldsymbol{\tau}^2 \end{aligned}$$

where $\tilde{\mathbf{w}}_l = (\|\bar{\mathbf{w}}_{l1}\|_2, \dots, \|\bar{\mathbf{w}}_{lk_{l+1}}\|_2)^T$ and the last inequality holds since for the first part, $\Pi(\|\tilde{\mathbf{w}}_l\|_0 > s_l^\circ | \boldsymbol{\tau}^2, \mathbf{z}) \leq 1$, $\Pi(\|\tilde{\mathbf{w}}_l\|_0 > s_l^\circ | \boldsymbol{\tau}^2, \mathbf{z}) = 1$ iff $\sum z_{li} > s_l^\circ$ and for the second part, $\pi(\mathbf{z}) \leq 1$. We will prove the inequality for each part separately.

Part 1. We direct the reader to Proof of Lemma 4.2 in Jantre et al. (2022) by which

$$\sum_{l=0}^L \mathbb{P}(\sum_{i=1}^{k_{l+1}} z_{li} > s_l^\circ) = \sum_{l=0}^L \mathbb{P}(\sum_{i=1}^{k_{l+1}} z_{li} - k_{l+1} \lambda_l > s_l^\circ - k_{l+1} \lambda_l).$$

Part 2.

$$\sum_{l=0}^L \int \mathbb{P}(\sup_{i=1, \dots, k_{l+1}} \|\mathbf{w}_{li}\|_2 > B_l^\circ | \boldsymbol{\tau}^2) \pi(\boldsymbol{\tau}^2) d\boldsymbol{\tau}^2 \leq \sum_{l=0}^L \sum_{i=1}^{k_{l+1}} \int \mathbb{P}(\|\mathbf{w}_{li}\|_2 > B_l^\circ | \tau_{li}^2) \pi(\tau_{li}^2) d\tau_{li}^2$$

$$\begin{aligned}
&\leq \sum_{l=0}^L \sum_{i=1}^{k_{l+1}} \int \mathbb{P}\left(\|\mathbf{w}_{li}\|_\infty > \frac{B_l^\circ}{k_l+1} \middle| \tau_{li}^2\right) \pi(\tau_{li}^2) d\tau_{li}^2 \\
&\leq \sum_{l=0}^L \sum_{i=1}^{k_{l+1}} \sum_{j=1}^{k_{l+1}} \int \mathbb{P}\left(|w_{lij}| > \frac{B_l^\circ}{k_l+1} \middle| \tau_{li}^2\right) \pi(\tau_{li}^2) d\tau_{li}^2 \\
&\leq 2 \sum_{l=0}^L \sum_{i=1}^{k_{l+1}} \sum_{j=1}^{k_{l+1}} \int \exp\left(-\frac{B_l^{\circ 2}}{2(k_l+1)^2 \tau_{li}^2}\right) \pi(\tau_{li}^2) d\tau_{li}^2 \quad \text{By concentration inequality} \\
&\leq 2 \sum_{l=0}^L \sum_{i=1}^{k_{l+1}} \sum_{j=1}^{k_{l+1}} \left[\exp\left(-\frac{\varsigma^2 B_l^\circ}{2(k_l+1)}\right) \mathbb{P}\left(\tau_{li}^2 \leq \frac{B_l^\circ}{\varsigma^2(k_l+1)}\right) + \mathbb{P}\left(\tau_{li}^2 \geq \frac{B_l^\circ}{\varsigma^2(k_l+1)}\right) \right] \\
&\leq 2 \sum_{l=0}^L \sum_{i=1}^{k_{l+1}} \sum_{j=1}^{k_{l+1}} \left[\exp\left(-\frac{\varsigma^2 B_l^\circ}{2(k_l+1)}\right) + \exp\left(-\frac{B_l^\circ}{k_l+1}\right) \right] \\
&\leq 4 \sum_{l=0}^L \sum_{i=1}^{k_{l+1}} \sum_{j=1}^{k_{l+1}} \exp\left(-\frac{\min(1, \varsigma^2) B_l^\circ}{2(k_l+1)}\right) \leq \sum_{l=0}^L \sum_{i=1}^{k_{l+1}} \sum_{j=1}^{k_{l+1}} \frac{1}{(L+1)k_{l+1}(k_l+1)} \exp(-n\epsilon_n^2)
\end{aligned}$$

where the fourth inequality holds since $|w_{lij}|$ given τ_{li}^2 is bound above by a $|N(0, \tau_{li}^2 \sigma_0^2)|$ random variable and we take $\sigma_0^2 = 1$ w.l.o.g. Moreover the above relation holds since $B_l^\circ = 2(n\epsilon_n^2 + \log(k_l+1) + \log k_{l+1} + \log(L+1) + \log 4)(k_l+1)/\min(1, \varsigma^2)$. \blacksquare

Proof of Lemma 11 Condition 1.

$$\text{Assumption : } -\log \lambda_l = O((k_l+1)\vartheta_l), \quad -\log(1-\lambda_l) = O(s_l(k_l+1)\vartheta_l/k_{l+1}) \quad (19)$$

Let $\sigma_\epsilon^2 = 1$ w.l.o.g. Then $P_0(y, \mathbf{x}) = \exp(-(y - \eta_0(\mathbf{x}))^2)/\sqrt{2\pi}$ and $P_\theta(y, \mathbf{x}) = \exp(-(y - \eta_\theta(\mathbf{x}))^2)/\sqrt{2\pi}$ which implies

$$2d_{\text{KL}}(P_0, P_\theta) = \int_{\mathbf{x} \in [0,1]^p} (\eta_0(\mathbf{x}) - \eta_\theta(\mathbf{x}))^2 d\mathbf{x} = \|\eta_0 - \eta_\theta\|_2^2 \quad (20)$$

Next, let $\eta_{\theta^*}(\mathbf{x})$ minimize $\eta_\theta \in \mathcal{F}(L, \mathbf{k}, \mathbf{s}, \mathbf{B}) \|\eta_\theta - \eta_0\|_\infty^2$

$$\|\eta_{\theta^*} - \eta_0\|_1 \leq \|\eta_{\theta^*} - \eta_0\|_\infty = \sqrt{\xi} \quad (21)$$

Here, we redefine $\bar{\mathbf{d}}_l$ by considering the L_2 norms of the rows of $\bar{\mathbf{D}}_l = \bar{\mathbf{W}}_l - \bar{\mathbf{W}}_l^*$ as follows $\bar{\mathbf{D}}_l = (\bar{\mathbf{d}}_{l1}^\top, \dots, \bar{\mathbf{d}}_{lk_{l+1}}^\top)^\top$ $\bar{\mathbf{d}}_l = (\|\bar{\mathbf{d}}_{l1}\|_2, \dots, \|\bar{\mathbf{d}}_{lk_{l+1}}\|_2)$. For \mathcal{S}_l^c is the set where $\|\bar{\mathbf{w}}_{li}^*\|_2 = 0$, $l = 0, \dots, L$, we define a neighborhood $\mathcal{M}_{\sqrt{\sum r_l}}$ as:

$$\mathcal{M}_{\sqrt{\sum r_l}} = \left\{ \theta : \|\bar{\mathbf{d}}_{li}\|_2 \leq \frac{\sqrt{\sum r_l} B_l}{(L+1)(\prod_{j=0}^L B_j)}, i \in \mathcal{S}_l, \|\bar{\mathbf{d}}_{li}\|_2 = 0, i \in \mathcal{S}_l^c, l = 0, \dots, L \right\}$$

For every $\theta \in \mathcal{M}_{\sqrt{\sum r_l}}$ by relation (16) in Jantre et al. (2022),

$$\|\eta_\theta - \eta_{\theta^*}\|_1 \leq \sqrt{\sum r_l} \quad (22)$$

Combining (21) and (22), for $\theta \in \mathcal{M}_{\sqrt{\sum r_l}}$, $\|\eta_\theta - \eta_0\|_1 \leq \sqrt{\sum r_l} + \sqrt{\xi}$, thus, $d_{\text{KL}}(P_0, P_\theta) \leq (\sqrt{\sum r_l} +$

$\sqrt{\xi})^2/2 \leq \sum r_l + \xi$. Since $\boldsymbol{\theta} \in \mathcal{N}_{\sum r_l + \xi}$ for every $\boldsymbol{\theta} \in \mathcal{M}_{\sqrt{\sum r_l}}$, $\int_{\boldsymbol{\theta} \in \mathcal{N}_{\sum r_l + \xi}} \tilde{\pi}(\boldsymbol{\theta}) d\boldsymbol{\theta} \geq \int_{\boldsymbol{\theta} \in \mathcal{M}_{\sqrt{\sum r_l}}} \tilde{\pi}(\boldsymbol{\theta}) d\boldsymbol{\theta}$. Let $\delta_n = (\sqrt{\sum r_l} B_l) / ((L+1)(\prod_{j=0}^L B_j))$, $A = \{\bar{\mathbf{w}}_{li} : \|\bar{\mathbf{w}}_{li} - \bar{\mathbf{w}}_{li}^*\|_2 \leq \delta_n\}$

$$\begin{aligned}
\tilde{\Pi}(\mathcal{M}_{\sqrt{\sum r_l}}) &= \int \sum_{\mathbf{z}} \Pi(\mathcal{M}_{\sqrt{\sum r_l}} | \boldsymbol{\tau}^2, \mathbf{z}) \pi(\mathbf{z}) \pi(\boldsymbol{\tau}^2) d\boldsymbol{\tau}^2 \\
&\geq \int \sum_{\{\mathbf{z}: z_{li}=1, i \in \mathcal{S}_l, z_{li}=0, i \in \mathcal{S}_l^c, l=0, \dots, L\}} \Pi(\mathcal{M}_{\sqrt{\sum r_l}} | \boldsymbol{\tau}^2, \mathbf{z}) \pi(\mathbf{z}) \pi(\boldsymbol{\tau}^2) d\boldsymbol{\tau}^2 \\
&= \prod_{l=0}^L (1 - \lambda_l)^{k_{l+1} - s_l} \lambda_l^{s_l} \prod_{i \in \mathcal{S}_l} \int \mathbb{E}(\mathbb{1}_{\{\bar{\mathbf{w}}_{li} \in A\}} | \tau_{li}^2, z_{li} = 1) \pi(\tau_{li}^2) d\tau_{li}^2 \\
&\geq \prod_{l=0}^L (1 - \lambda_l)^{k_{l+1} - s_l} \lambda_l^{s_l} \prod_{i \in \mathcal{S}_l} \mathbb{E}(\mathbb{1}_{\{\bar{\mathbf{w}}_{li} \in A\}} | \tau_{li}^2 = (k_l + 1)/\varsigma^2, z_{li} = 1) \mathbb{P}(\tau_{li}^2 \leq (k_l + 1)/\varsigma^2) \\
&= \prod_{l=0}^L (1 - \lambda_l)^{k_{l+1} - s_l} \lambda_l^{s_l} \prod_{i \in \mathcal{S}_l} \int_{\bar{\mathbf{w}}_{li} \in A} \left(\frac{\varsigma^2}{2\pi(k_l + 1)} \right)^{\frac{k_l+1}{2}} \prod_{j=1}^{k_l+1} \exp\left(-\frac{\varsigma^2 \bar{w}_{lij}^2}{2(k_l + 1)}\right) d\bar{w}_{lij} \\
&\quad \times \mathbb{P}(\tau_{li}^2 \leq (k_l + 1)/\varsigma^2) \\
&\geq \prod_{l=0}^L (1 - \lambda_l)^{k_{l+1} - s_l} \lambda_l^{s_l} \left[\prod_{i \in \mathcal{S}_l} \left(\frac{\varsigma^2}{2\pi(k_l + 1)} \right)^{\frac{k_l+1}{2}} \prod_{j=1}^{k_l+1} \int_{\bar{w}_{lij}^* - \frac{\delta_n}{\sqrt{k_l+1}}}^{\bar{w}_{lij}^* + \frac{\delta_n}{\sqrt{k_l+1}}} \exp\left(-\frac{\varsigma^2 \bar{w}_{lij}^2}{2(k_l + 1)}\right) d\bar{w}_{lij} \right] \\
&\quad \times (1 - \exp(-s_l(k_l + 1)/2)) \\
&\geq \prod_{l=0}^L (1 - \lambda_l)^{k_{l+1} - s_l} \lambda_l^{s_l} \left[\prod_{i \in \mathcal{S}_l} \left(\frac{\varsigma^2}{2\pi(k_l + 1)} \right)^{\frac{k_l+1}{2}} \prod_{j=1}^{k_l+1} \frac{2\delta_n}{\sqrt{k_l + 1}} \exp\left(-\frac{\hat{w}_{lij}^2 \varsigma^2}{2(k_l + 1)}\right) \right] \\
&\quad \times (1 - \exp(-s_l(k_l + 1)/2))
\end{aligned}$$

where third equality holds since $\mathbb{E}(\mathbb{1}_{\{\bar{\mathbf{w}}_{li} \in A\}} | \tau_{li}^2 = (k_l + 1)/\varsigma^2, z_{li} = 0) = 1$, $\|\bar{\mathbf{w}}_{li}^*\|_2 = 0$, for $i \in \mathcal{S}_l^c$. The last equality is by mean value theorem and $\hat{w}_{lij} \in [\bar{w}_{lij}^* - \delta_n/(k_l + 1), \bar{w}_{lij}^* + \delta_n/(k_l + 1)]$

$$\begin{aligned}
&= \exp \left[- \sum_{l=0}^L \left\{ s_l \log\left(\frac{1}{\lambda_l}\right) + (k_{l+1} - s_l) \log\left(\frac{1}{1 - \lambda_l}\right) \right. \right. \\
&\quad \left. \left. + \sum_{i \in \mathcal{S}_l} \left(-\frac{k_l + 1}{2} \log \frac{\varsigma^2}{2\pi(k_l + 1)} - (k_l + 1) \log \frac{2\delta_n}{\sqrt{k_l + 1}} + \sum_{j=1}^{k_l+1} \frac{\hat{w}_{lij}^2 \varsigma^2}{2(k_l + 1)} + \frac{(k_l + 1)}{2} \right) \right\} \right] \\
&= \exp \left[- \sum_{l=0}^L \left\{ s_l \log\left(\frac{1}{\lambda_l}\right) + (k_{l+1} - s_l) \log\left(\frac{1}{1 - \lambda_l}\right) + \frac{s_l(k_l + 1)}{2} (1 + \log(2\pi)) \right. \right. \\
&\quad \left. \left. + s_l(k_l + 1) \left(\frac{1}{2} \log \frac{(k_l + 1)}{\varsigma^2} + \frac{1}{2} \log(k_l + 1) - \log(2\delta_n) \right) + \sum_{i \in \mathcal{S}_l} \sum_{j=1}^{k_l+1} \frac{\hat{w}_{lij}^2 \varsigma^2}{2(k_l + 1)} \right\} \right] \tag{23}
\end{aligned}$$

Using $\delta_n \rightarrow 0$, we get

$$\frac{\varsigma^2}{2} \sum_{l=0}^L \sum_{i \in \mathcal{S}_l} \sum_{j=1}^{k_l+1} \frac{\hat{w}_{lij}^2}{k_l + 1} \leq \frac{\varsigma^2}{2} \sum_{l=0}^L \sum_{i \in \mathcal{S}_l} \sum_{j=1}^{k_l+1} \frac{(\max((\bar{w}_{lij}^* - \delta_n/\sqrt{k_l+1}), (\bar{w}_{lij}^* + \delta_n/\sqrt{k_l+1})))^2}{k_l + 1}$$

$$\leq \varsigma^2 \sum_{l=0}^L \sum_{i \in \mathcal{S}_l} \sum_{j=1}^{k_l+1} \frac{\bar{w}_{lij}^{*2} + \delta_n^2 / (k_l + 1)}{k_l + 1} \leq \sum_{l=0}^L s_l (k_l + 1) \left(\frac{B_l^2}{(k_l + 1)} + \frac{1}{(k_l + 1)} \right) \frac{\varsigma^2}{k_l + 1} \quad (24)$$

$$\begin{aligned} & \sum_{l=0}^L \left(s_l \log \left(\frac{1}{\lambda_l} \right) + (k_{l+1} - s_l) \log \left(\frac{1}{1 - \lambda_l} \right) + \frac{s_l (k_l + 1)}{2} \left(\log(k_l + 1)^3 - 2 \log(2\varsigma \delta_n \sqrt{2\pi e}) \right) \right) \\ & \sim \sum_{l=0}^L \left(s_l \log \left(\frac{1}{\lambda_l} \right) + (k_{l+1} - s_l) \log \left(\frac{1}{1 - \lambda_l} \right) \right) \\ & + \sum_{l=0}^L \frac{s_l (k_l + 1)}{2} \left(2 \log(k_l + 1) - \log \varsigma^2 + 2 \log(L + 1) + 2 \sum \log B_m - \log B_l^2 - \log \sum r_l \right) \\ & \leq \sum_{l=0}^L C n r_l + \sum_{l=0}^L \frac{s_l (k_l + 1)}{2} \left(-\log \frac{B_l^2 \varsigma^2}{(k_l + 1)^2} + \log(L + 1) + 2 \sum \log B_m + \log n \right) \\ & \leq \sum_{l=0}^L C n r_l \end{aligned} \quad (25)$$

where the first inequality follows from (19) and expanding δ_n . The last inequality follows since $n \sum r_l \rightarrow \infty$. Combining (24) and (25) gives the bound for (23). \blacksquare

Proof of Lemma 11 Condition 2.

$$\text{Assumption : } -\log \lambda_l = O\{(k_l + 1)\vartheta_l\}, \quad -\log(1 - \lambda_l) = O\{(s_l/k_{l+1})(k_l + 1)\vartheta_l\}$$

Suppose there exists $q^* \in \mathcal{Q}$ such that

$$d_{\text{KL}}(q^*, \pi) \leq C_1 n \sum r_l \quad \sum_{\mathbf{z}} \int_{\boldsymbol{\theta}} \|\eta_{\boldsymbol{\theta}} - \eta_{\boldsymbol{\theta}^*}\|_2^2 q^*(\boldsymbol{\theta}, \mathbf{z}) d\boldsymbol{\theta} \leq \sum r_l. \quad (26)$$

Recall $\boldsymbol{\theta}^* = \arg \min_{\boldsymbol{\theta}: \eta_{\boldsymbol{\theta}} \in \mathcal{F}(L, p, s, \mathbf{B})} \|\eta_{\boldsymbol{\theta}} - \eta_0\|_{\infty}^2$. By relation (20),

$$\begin{aligned} \sum_{\mathbf{z}} \int n d_{\text{KL}}(P_0, P_{\boldsymbol{\theta}}) q^*(\boldsymbol{\theta}, \mathbf{z}) d\boldsymbol{\theta} & \leq \frac{n}{2} \left(\sum_{\mathbf{z}} \int \|\eta_{\boldsymbol{\theta}^*} - \eta_{\boldsymbol{\theta}}\|_2^2 q^*(\boldsymbol{\theta}, \mathbf{z}) d\boldsymbol{\theta} + \frac{n}{2} \|\eta_{\boldsymbol{\theta}^*} - \eta_0\|_{\infty}^2 \right) \\ & \leq C n (\sum r_l + \xi) \end{aligned}$$

where the above relation is due to (26). Next we construct q^* as

$$\bar{w}_{lij} | z_i^* \sim z_i^* \mathcal{N}(\bar{w}_{lij}^*, \sigma_l^2) + (1 - z_i^*) \delta_0, \quad z_i^* \sim \text{Bern}(\gamma_{li}^*) \quad \gamma_{li}^* = \mathbb{1}(\|\mathbf{w}_{li}^*\|_2 \neq 0)$$

where $\sigma_l^2 = \frac{s_l^*}{8n(L+1)} (4^{L-l} (k_l + 1) \log(s_l^* 2^{k_l+1}) \prod_{m=0, m \neq l}^L B_m^2)^{-1}$. For this choice of q^* , we have $\int \|\eta_{\boldsymbol{\theta}} - \eta_{\boldsymbol{\theta}^*}\|_2^2 q^*(\boldsymbol{\theta}, \mathbf{z}) d\boldsymbol{\theta} \leq \sum r_l$. The proof of this follows as a consequence of Proof of Lemma 4.3 part 2. in Jantre et al. (2022). Next, $d_{\text{KL}}(q^*, \pi)$ is bounded above by

$$\log \frac{1}{\pi(\mathbf{z}^*)} + \mathbb{1}(\mathbf{z} = \mathbf{z}^*) \int \dots \int d_{\text{KL}} \left(\left\{ \prod_{l=0}^{L-1} \prod_{i=1}^{k_{l+1}} \prod_{j=1}^{k_l+1} \left\{ z_{li} \mathcal{N}(\bar{w}_{lij}^*, \sigma_l^2) + (1 - z_{li}) \delta_0 \right\} \right\} \right)$$

$$\begin{aligned}
& \prod_{j=1}^{k_L+1} \mathcal{N}(\bar{w}_{Lj}^*, \sigma_L^2) \Big\}, \left\{ \prod_{l=0}^{L-1} \prod_{i=1}^{k_{l+1}} \prod_{j=1}^{k_{l+1}} \left\{ z_{li} \mathcal{N}(0, \sigma_0^2 \tau_{li}^2) + (1 - z_{li}) \delta_0 \right\} \prod_{j=1}^{k_L+1} \mathcal{N}(0, \sigma_0^2 \tau_L^2) \right\} \\
& \prod_{l,i} LN \left(\mu_{li}^{\{\tau\}}, \sigma_{li}^{\{\tau\}2} \right) d\tau_{li}^2 + \sum_{l,i} d_{\text{KL}} \left(LN \left(\mu_{li}^{\{\tau\}}, \sigma_{li}^{\{\tau\}2} \right), \Gamma \left(\frac{k_l + 2}{2}, \frac{\zeta^2}{2} \right) \right) \\
& = \sum_{l=0}^{L-1} \left(s_l^* \log \frac{1}{\lambda_l} + (k_{l+1} - s_l^*) \log \frac{1}{1 - \lambda_l} \right) \\
& \quad + \sum_{l=0}^{L-1} \sum_{i=1}^{k_{l+1}} z_{li} \sum_{j=1}^{k_{l+1}} \left\{ \frac{1}{2} \log \frac{\sigma_0^2}{\sigma_l^2} + \frac{1}{2} \mu_{li}^{\{\tau\}} + \frac{\sigma_l^2 + \bar{w}_{lij}^{*2}}{2\sigma_0^2} \exp \left(-\mu_{li}^{\{\tau\}} + \frac{\sigma_{li}^{\{\tau\}2}}{2} \right) - \frac{1}{2} \right\} \\
& \quad + \sum_{j=1}^{k_L+1} \left\{ \frac{1}{2} \log \frac{\sigma_0^2}{\sigma_L^2} + \frac{1}{2} \mu_L^{\{\tau\}} + \frac{\sigma_L^2 + \bar{w}_{Lj}^{*2}}{2\sigma_0^2} \exp \left(-\mu_L^{\{\tau\}} + \frac{\sigma_L^{\{\tau\}2}}{2} \right) - \frac{1}{2} \right\} \\
& \quad + \sum_{l=0}^L \sum_{i=1}^{k_{l+1}} \left[\frac{k_l + 2}{2} \log 2 - \frac{k_l + 2}{2} \log \zeta^2 + \log \Gamma \left(\frac{k_l + 2}{2} \right) - \frac{k_l + 2}{2} \mu_{li}^{\{\tau\}} \right. \\
& \quad \quad \left. + \frac{\zeta^2}{2} \exp \left(\mu_{li}^{\{\tau\}} + \frac{\sigma_{li}^{\{\tau\}2}}{2} \right) - \log \sigma_{li}^{\{\tau\}} - \log \sqrt{2\pi} - \frac{1}{2} \right] \\
& \leq \sum_{l=0}^{L-1} Cnr_l + \frac{k_L + 1}{2} \left[\mu_L^{\{\tau\}} + \left\{ \frac{\sigma_L^2}{\sigma_0^2} + \frac{B_L^2}{\sigma_0^2(k_L + 1)} \right\} \exp \left(-\mu_L^{\{\tau\}} + \frac{\sigma_L^{\{\tau\}2}}{2} \right) - 1 + \log \frac{\sigma_0^2}{\sigma_L^2} \right] \\
& \quad + \sum_{l=0}^{L-1} \sum_{i=1}^{s_i^*} \frac{k_l + 1}{2} \left[\mu_{li}^{\{\tau\}} + \left\{ \frac{\sigma_l^2}{\sigma_0^2} + \frac{B_l^2}{\sigma_0^2(k_l + 1)} \right\} \exp \left(-\mu_{li}^{\{\tau\}} + \frac{\sigma_{li}^{\{\tau\}2}}{2} \right) - 1 + \log \frac{\sigma_0^2}{\sigma_l^2} \right] \\
& \quad + \sum_{l=0}^L \sum_{i=1}^{k_{l+1}} \left[\frac{k_l + 2}{2} \log 2 - \frac{k_l + 2}{2} \log \zeta^2 + \log \Gamma \left(\frac{k_l + 2}{2} \right) - \frac{k_l + 2}{2} \mu_{li}^{\{\tau\}} \right. \\
& \quad \quad \left. + \frac{\zeta^2}{2} \exp \left(\mu_{li}^{\{\tau\}} + \frac{\sigma_{li}^{\{\tau\}2}}{2} \right) - \log \sigma_{li}^{\{\tau\}} - \log \sqrt{2\pi} - \frac{1}{2} \right]
\end{aligned}$$

The first line follows from Lemma A.4 in Jantre et al. (2022). The last inequality follows from $\sum_{j=1}^{k_l+1} \bar{w}_{lij}^{*2} \leq B_l^2$ and (19). Note, $\sigma_0^2 = 1$, $\sigma_l^2 \leq 1$. Let $b_l = (k_l + 1) \log(k_{l+1} 2^{k_l+1})$ and $d_l = \prod_{m=0, m \neq l}^L B_m^2$. Let $\exp(\mu_{li}^{\{\tau\}} + \sigma_{li}^{\{\tau\}2}/2) = (k_l + 2)/\zeta^2$ and $\exp(\sigma^2) = 1 + 2/(k_l + 2)$.

$$\begin{aligned}
& d_{\text{KL}}(q, \pi) \\
& \leq \sum_{l=0}^{L-1} Cnr_l + \frac{k_L + 1}{2} \left[\mu_L^{\{\tau\}} + \left\{ \sigma_L^2 + \frac{B_L^2}{(k_L + 1)} \right\} \exp \left(-\mu_L^{\{\tau\}} + \frac{\sigma_L^{\{\tau\}2}}{2} \right) - 1 - \log \sigma_L^2 \right] \\
& \quad + \sum_{l=0}^{L-1} \sum_{i=1}^{s_i^*} \frac{k_l + 1}{2} \left[\mu_{li}^{\{\tau\}} + \left\{ \sigma_l^2 + \frac{B_l^2}{(k_l + 1)} \right\} \exp \left(-\mu_{li}^{\{\tau\}} + \frac{\sigma_{li}^{\{\tau\}2}}{2} \right) - 1 - \log \sigma_l^2 \right] \\
& \quad + \sum_{l=0}^L \sum_{i=1}^{k_{l+1}} \left[\frac{k_l + 2}{2} \log 2 - \frac{k_l + 2}{2} \log \zeta^2 + \log \Gamma \left(\frac{k_l + 2}{2} \right) - \frac{k_l + 2}{2} \mu_{li}^{\{\tau\}} - \frac{1}{2} \right. \\
& \quad \quad \left. + \frac{\zeta^2}{2} \exp \left(\mu_{li}^{\{\tau\}} + \frac{\sigma_{li}^{\{\tau\}2}}{2} \right) - \log \sigma_{li}^{\{\tau\}} - \log \sqrt{2\pi} \right]
\end{aligned}$$

$$\begin{aligned}
&\leq \sum_{l=0}^{L-1} Cnr_l + \frac{k_L+1}{2} \left(\log \frac{k_L+2}{\varsigma^2} + \left\{ 1 + \frac{B_L^2}{(k_L+1)} \right\} \frac{\varsigma^2}{k_L+2} - \log \sigma_L^2 \right) \\
&+ \sum_{l=0}^{L-1} \frac{s_l^*(k_l+1)}{2} \left(\log \frac{k_l+2}{\varsigma^2} + \left\{ 1 + \frac{B_l^2}{(k_l+1)} \right\} \frac{\varsigma^2}{k_l+2} - \log \sigma_l^2 \right) + C_1 L \\
&\leq \sum_{l=0}^{L-1} Cnr_l + \frac{k_L+1}{2} \left[\log \frac{k_L+2}{\varsigma^2} + \left(1 + \frac{B_L^2}{(k_L+1)} \right) \frac{\varsigma^2}{(k_L+2)} - \log \left(\frac{1}{8n(L+1)b_L d_L} \right) \right] \\
&+ \sum_{l=0}^{L-1} \frac{s_l^*(k_l+1)}{2} \left[\log \frac{k_l+2}{\varsigma^2} + \left(1 + \frac{B_l^2}{(k_l+1)} \right) \frac{\varsigma^2}{k_l+2} - \log \left(\frac{s_l^*}{8n(L+1)4^{L-l} b_l d_l} \right) \right] \\
&\leq \sum_{l=0}^L Cnr_l + \sum_{l=0}^L \frac{s_l^*(k_l+1)}{2} \left[\log \frac{k_l+2}{\varsigma^2} + \left(1 + \frac{B_l^2}{(k_l+1)} \right) \frac{\varsigma^2}{k_l+2} - \log B_l^2 \right. \\
&\quad \left. - \log s_l^* + L \log 2 + \log n + \log 8 + \log \log s_l^* + \log(k_l+1) + 2 \sum \log B_m \right] \\
&\leq \sum_{l=0}^L Cnr_l + \sum_{l=0}^L \frac{s_l^*(k_l+1)}{2} \left[\log \frac{k_l+2}{\varsigma^2} + \left(1 + \frac{B_l^2}{(k_l+1)} \right) \frac{\varsigma^2}{k_l+2} - \log \frac{B_l^2}{k_l+1} \right. \\
&\quad \left. + 2L + 2 \log n + 2 \sum \log B_m \right] \leq \sum_{l=0}^L Cnr_l \quad \blacksquare
\end{aligned}$$

D Spike-and-Slab Group Horseshoe Proofs

Proof of Lemma 10.

The proof of part-1 is same as SS-GL. We prove part-2 for SS-GHS below.

$$\begin{aligned}
\tilde{\Pi}(\mathcal{F}(L, \mathbf{k}, \mathbf{s}^\circ, \mathbf{B}^\circ)^c) &\leq \tilde{\Pi} \left(\bigcup_{l=0}^L \{ \|\tilde{\mathbf{w}}_l\|_0 > s_l^\circ \} \right) + \tilde{\Pi} \left(\bigcup_{l=0}^L \{ \|\tilde{\mathbf{w}}_l\|_\infty > B_l^\circ \} \right) \\
&\leq \sum_{l=0}^L \tilde{\Pi}(\|\tilde{\mathbf{w}}_l\|_0 > s_l^\circ) + \sum_{l=0}^L \tilde{\Pi}(\|\tilde{\mathbf{w}}_l\|_\infty > B_l^\circ) \\
&= \sum_{l=0}^L \int \int \sum_{\mathbf{z}} \Pi(\|\tilde{\mathbf{w}}_l\|_0 > s_l^\circ | \boldsymbol{\tau}^2, s^2, \mathbf{z}) \pi(\mathbf{z}) \pi(\boldsymbol{\tau}^2) \pi(s^2) d\boldsymbol{\tau}^2 ds^2 \\
&\quad + \sum_{l=0}^L \int \int \sum_{\mathbf{z}} \Pi(\|\tilde{\mathbf{w}}_l\|_\infty > B_l^\circ | \boldsymbol{\tau}^2, s^2, \mathbf{z}) \pi(\mathbf{z}) \pi(\boldsymbol{\tau}^2) \pi(s^2) d\boldsymbol{\tau}^2 ds^2 \\
&\leq \sum_{l=0}^L \mathbb{P} \left(\sum_{i=1}^{k_{l+1}} z_{li} > s_l^\circ \right) + \sum_{l=0}^L \int \int \mathbb{P} \left(\sup_{i=1, \dots, k_{l+1}} \|\bar{\mathbf{w}}_{li}\|_2 > B_l^\circ \mid \boldsymbol{\tau}^2, s^2 \right) \pi(\boldsymbol{\tau}^2) \pi(s^2) d\boldsymbol{\tau}^2 ds^2
\end{aligned}$$

Part 2.

$$\sum_{l=0}^L \int \mathbb{P} \left(\sup_{i=1, \dots, k_{l+1}} \|\mathbf{w}_{li}\|_2 > B_l^\circ \mid \boldsymbol{\tau}^2, s^2 \right) \pi(\boldsymbol{\tau}^2) d\boldsymbol{\tau}^2 \pi(s^2) ds^2$$

$$\begin{aligned}
&\leq \sum_{l=0}^L \sum_{i=1}^{k_{l+1}} \int \int \mathbb{P}(\|\mathbf{w}_{li}\|_2 > B_l^\circ | \tau_{li}^2, s^2) \pi(\tau_{li}^2) d\tau_{li}^2 \pi(s^2) ds^2 \\
&\leq \sum_{l=0}^L \sum_{i=1}^{k_{l+1}} \int \int \mathbb{P}\left(\|\mathbf{w}_{li}\|_\infty > \frac{B_l^\circ}{k_l + 1} \middle| \tau_{li}^2, s^2\right) \pi(\tau_{li}^2) d\tau_{li}^2 \pi(s^2) ds^2 \\
&\leq \sum_{l=0}^L \sum_{i=1}^{k_{l+1}} \int \int \sum_{j=1}^{k_{l+1}} \mathbb{P}\left(|w_{lij}| > \frac{B_l^\circ}{k_l + 1} \middle| \tau_{li}^2, s^2\right) \pi(\tau_{li}^2) d\tau_{li}^2 \pi(s^2) ds^2 \\
&\leq 2 \sum_{l=0}^L \sum_{i=1}^{k_{l+1}} \int \int \sum_{j=1}^{k_{l+1}} \exp\left(-\frac{B_l^{\circ 2}(c^2 + \tau_{li}^2 s^2)}{2(k_l + 1)^2 c^2 \tau_{li}^2 s^2}\right) \pi(\tau_{li}^2) d\tau_{li}^2 \pi(s^2) ds^2 \\
&\leq 2 \sum_{l=0}^L \sum_{i=1}^{k_{l+1}} \sum_{j=1}^{k_{l+1}} \exp\left(-\frac{B_l^{\circ 2}}{2c^2(k_l + 1)^2}\right) \leq \sum_{l=0}^L \sum_{i=1}^{k_{l+1}} \sum_{j=1}^{k_{l+1}} \frac{1}{(L+1)k_{l+1}(k_l + 1)} \exp(-n\epsilon_n^2)
\end{aligned}$$

where the fourth inequality holds because $|w_{lij}|$ given τ_{li}^2 and s^2 is bound above by a $|N(0, \frac{c^2 \tau_{li}^2 s^2 \sigma_0^2}{c^2 + \tau_{li}^2 s^2})|$ random variable and we take $\sigma_0^2 = 1$ w.l.o.g. Moreover, the above proof holds since $(B_l^\circ)^2 = 2(n\epsilon_n^2 + \log(k_l + 1) + \log k_{l+1} + \log(L+1) + \log 2)(k_l + 1)^2 c^2$. \blacksquare

Proof of Lemma 11 Condition 1.

$$Assumption : -\log \lambda_l = O\{(k_l + 1)\vartheta_l\}, \quad -\log(1 - \lambda_l) = O\{(s_l/k_{l+1})(k_l + 1)\vartheta_l\} \quad (27)$$

The initial parts of the proof are the same as the SS-GL and below we detail the remaining parts of the proof which differ from SS-GL in the SS-GHS case.

Let $\delta_n = (\sqrt{\sum r_l B_l}) / ((L+1)(\prod_{j=0}^L B_j))$ and $A = \{\bar{\mathbf{w}}_{li} : \|\bar{\mathbf{w}}_{li} - \bar{\mathbf{w}}_{li}^*\|_2 \leq \delta_n\}$

$$\begin{aligned}
\tilde{\Pi}(\mathcal{M}_{\sqrt{\sum r_l}}) &= \int \int \sum_{\mathbf{z}} \Pi(\mathcal{M}_{\sqrt{\sum r_l}} | \boldsymbol{\tau}^2, s^2, \mathbf{z}) \pi(\mathbf{z}) \pi(\boldsymbol{\tau}^2) \pi(s^2) d\boldsymbol{\tau}^2 ds^2 \\
&\geq \int \int \sum_{\{\mathbf{z}: z_{li}=1, i \in \mathcal{S}_l, z_{li}=0, i \in \mathcal{S}_l^c, l=0, \dots, L\}} \Pi(\mathcal{M}_{\sqrt{\sum r_l}} | \boldsymbol{\tau}^2, s^2, \mathbf{z}) \pi(\mathbf{z}) \pi(\boldsymbol{\tau}^2) \pi(s^2) d\boldsymbol{\tau}^2 ds^2 \\
&= \prod_{l=0}^L (1 - \lambda_l)^{k_{l+1} - s_l} \lambda_l^{s_l} \int \prod_{i=1}^{k_{l+1}} \int \mathbb{E}(\mathbb{1}_{\{\bar{\mathbf{w}}_{li} \in A\}} | \tau_{li}^2, s^2, z_{li} = 1) \pi(\tau_{li}^2) \pi(s^2) d\tau_{li}^2 ds^2 \\
&= \prod_{l=0}^L (1 - \lambda_l)^{k_{l+1} - s_l} \lambda_l^{s_l} \int_0^\infty \prod_{i \in \mathcal{S}_l} \int_0^\infty \int_{\bar{\mathbf{w}}_{li} \in A} \left[\left(\frac{c^2 + \tau_{li}^2 s^2}{2\pi c^2 \tau_{li}^2 s^2} \right)^{\frac{k_{l+1}}{2}} \right. \\
&\quad \times \prod_{j=1}^{k_{l+1}} \exp\left(-\frac{\bar{w}_{lij}^2 (c^2 + \tau_{li}^2 s^2)}{2c^2 \tau_{li}^2 s^2}\right) d\bar{w}_{lij} \pi(\tau_{li}^2) \pi(s^2) d\tau_{li}^2 ds^2 \\
&\geq \prod_{l=0}^L \left\{ (1 - \lambda_l)^{k_{l+1} - s_l} \lambda_l^{s_l} \int_0^\infty \left[\prod_{i \in \mathcal{S}_l} \left(\frac{1 + \tau_{li}^2 s^2 / c^2}{2\pi} \right)^{\frac{k_{l+1}}{2}} \int_0^\infty \left[\int_{\bar{w}_{lij}^* - \frac{\delta_n}{\sqrt{k_{l+1}}} }^{\bar{w}_{lij}^* + \frac{\delta_n}{\sqrt{k_{l+1}}} } \prod_{j=1}^{k_{l+1}} \right. \right. \right. \\
&\quad \left. \left. \left. \exp\left(-\frac{\bar{w}_{lij}^2 (c^2 + \tau_{li}^2 s^2)}{2c^2 \tau_{li}^2 s^2}\right) d\bar{w}_{lij} \right] K(\tau_{li}^2)^{-\frac{k_{l+1}}{2} - a - 1} L(\tau_{li}^2) d\tau_{li}^2 \right] K'(s^2)^{-\frac{s_l(k_{l+1})}{2} - a' - 1} L(s^2) ds^2 \right\}
\end{aligned}$$

$$\begin{aligned}
&\geq \prod_{l=0}^L \left\{ (1 - \lambda_l)^{k_{l+1} - s_l} \lambda_l^{s_l} \left[\prod_{i \in \mathcal{S}_l} \left(\frac{1 + t_0 t'_0 / c^2}{2\pi} \right)^{\frac{k_l+1}{2}} c_0 K \left(\frac{2\delta_n}{\sqrt{k_l+1}} \right)^{k_l+1} \right. \right. \\
&\quad \left. \left. \exp \left(- \sum_{j=1}^{k_l+1} \widehat{w}_{lij}^2 \left(\frac{1}{c^2} + \frac{1}{t_0 t'_0} \right) \right) \int_{t_0}^{\infty} (\tau_{li}^2)^{-\frac{k_l+1}{2} - a - 1} d\tau_{li}^2 \right] K' c'_0 \int_{t'_0}^{\infty} (s^2)^{-\frac{s_l(k_l+1)}{2} - a' - 1} ds^2 \right\} \\
&= \prod_{l=0}^L \left\{ (1 - \lambda_l)^{k_{l+1} - s_l} \lambda_l^{s_l} \int_0^{\infty} \left[\prod_{i \in \mathcal{S}_l} \left(\frac{1 + t_0 t'_0 / c^2}{2\pi} \right)^{\frac{k_l+1}{2}} \left(\frac{2\delta_n}{\sqrt{k_l+1}} \right)^{k_l+1} K c_0 \right. \right. \\
&\quad \left. \left. \exp \left(- \sum_{j=1}^{k_l+1} \widehat{w}_{lij}^2 \left(\frac{1}{c^2} + \frac{1}{t_0 t'_0} \right) \right) \frac{t_0^{-\frac{k_l+1}{2} - a}}{\frac{k_l+1}{2} + a} \right] K' c'_0 \frac{t_0^{-\frac{s_l(k_l+1)}{2} - a'}}{\frac{s_l(k_l+1)}{2} + a'} \right\}
\end{aligned}$$

where the third equality follows $\mathbb{E}(\mathbb{1}_{\{\overline{\mathbf{w}}_{li} \in A\}} | \tau_{li}^2, s^2, z_{li} = 0) = 1$ since $\|\overline{\mathbf{w}}_{li}^*\|_2 = 0$, for $i \in \mathcal{S}_l^c$. The last equality is by mean value theorem and $\widehat{w}_{lij} \in [\overline{w}_{lij}^* - \delta_n / \sqrt{k_l+1}, \overline{w}_{lij}^* + \delta_n / \sqrt{k_l+1}]$,

$$\begin{aligned}
&= \exp \left[- \sum_{l=0}^L \left\{ s_l \log \left(\frac{1}{\lambda_l} \right) + (k_{l+1} - s_l) \log \left(\frac{1}{1 - \lambda_l} \right) - C' - \frac{s_l(k_l+1)}{2} \log \left(1 + \frac{t_0 t'_0}{c^2} \right) \right. \right. \\
&\quad \left. \left. + \left(\frac{s_l(k_l+1)}{2} + a' \right) \log t'_0 + \log \left(\frac{s_l(k_l+1)}{2} + a' \right) + \frac{s_l(k_l+1)}{2} \log 2\pi + \sum_{i \in \mathcal{S}_l} \left(-C \right. \right. \right. \\
&\quad \left. \left. \left. - (k_l+1) \log \frac{2\delta_n}{\sqrt{k_l+1}} + \log t_0^{\frac{(k_l+1)}{2} + a} + \log \left(\frac{(k_l+1)}{2} + a \right) + \sum_{j=1}^{k_l+1} \widehat{w}_{lij}^2 \left(\frac{1}{t_0 t'_0} + \frac{1}{c^2} \right) \right) \right\} \right] \\
&\gtrsim \exp \left[- \sum_{l=0}^L \left\{ s_l \log \left(\frac{1}{\lambda_l} \right) + (k_{l+1} - s_l) \log \left(\frac{1}{1 - \lambda_l} \right) - \frac{s_l(k_l+1)}{2} \log \left(1 + \frac{t_0 t'_0}{c^2} \right) \right. \right. \\
&\quad \left. \left. + \left(\frac{s_l(k_l+1)}{2} + a' \right) \log t'_0 + \log \left(\frac{s_l(k_l+1)}{2} + a' \right) + \frac{s_l(k_l+1)}{2} \left(\log 2\pi - 2 \log \frac{2\delta_n}{\sqrt{k_l+1}} \right) \right. \right. \\
&\quad \left. \left. + s_l \left(\frac{k_l+1}{2} + a \right) \log t_0 + s_l \log \left(\frac{k_l+1}{2} + a \right) + \sum_{i \in \mathcal{S}_l} \sum_{j=1}^{k_l+1} \widehat{w}_{lij}^2 \left(\frac{1}{t_0 t'_0} + \frac{1}{c^2} \right) \right\} \right] \\
&\gtrsim \exp \left[- \sum_{l=0}^L \left\{ s_l \log \left(\frac{1}{\lambda_l} \right) + (k_{l+1} - s_l) \log \left(\frac{1}{1 - \lambda_l} \right) - \frac{s_l(k_l+1)}{2} \log \left(\frac{1}{t_0 t'_0} + \frac{1}{c^2} \right) \right. \right. \\
&\quad \left. \left. + \frac{s_l(k_l+1)}{2} \left(\log(k_l+1) - \log(\delta_n^2) \right) + \sum_{i \in \mathcal{S}_l} \sum_{j=1}^{k_l+1} \widehat{w}_{lij}^2 \left(\frac{1}{t_0 t'_0} + \frac{1}{c^2} \right) \right\} \right] \tag{28}
\end{aligned}$$

Here, $\sum_{l=0}^L \sum_{i \in \mathcal{S}_l} \sum_{j=1}^{k_l+1} \widehat{w}_{lij}^2 \left(\frac{1}{t_0 t'_0} + \frac{1}{c^2} \right)$ is bounded above by

$$\begin{aligned}
&\left(\frac{1}{t_0 t'_0} + \frac{1}{c^2} \right) \sum_{l=0}^L \sum_{i \in \mathcal{S}_l} \sum_{j=1}^{k_l+1} \max \left(\left(\overline{w}_{lij}^* - \frac{\delta_n}{\sqrt{k_l+1}} \right)^2, \left(\overline{w}_{lij}^* + \frac{\delta_n}{\sqrt{k_l+1}} \right)^2 \right) \\
&\leq 2 \left(\frac{1}{t_0 t'_0} + \frac{1}{c^2} \right) \sum_{l=0}^L \sum_{i \in \mathcal{S}_l} \sum_{j=1}^{k_l+1} \left(\overline{w}_{lij}^{*2} + \delta_n^2 / (k_l+1) \right) \\
&\leq \sum_{l=0}^L \sum_{i \in \mathcal{S}_l} 2 \|\overline{\mathbf{w}}_{li}^*\|_2^2 \left(\frac{1}{t_0 t'_0} + \frac{1}{c^2} \right) + \sum_{l=0}^L \sum_{i \in \mathcal{S}_l} \frac{2\delta_n^2}{(k_l+1)} \left(\frac{1}{t_0 t'_0} + \frac{1}{c^2} \right)
\end{aligned}$$

$$\leq \sum_{l=0}^L 2s_l(k_l+1) \left(\frac{B_l^2}{k_l+1} + \frac{1}{(k_l+1)} \right) \left(\frac{1}{t_0 t_0'} + \frac{1}{c^2} \right), \text{ since } \delta_n \rightarrow 0. \quad (29)$$

$$\begin{aligned} & \sum_{l=0}^L \left(s_l \log \left(\frac{1}{\lambda_l} \right) + (k_{l+1} - s_l) \log \left(\frac{1}{1 - \lambda_l} \right) - \frac{s_l(k_l+1)}{2} \left(\log \left(\frac{1}{t_0 t_0'} + \frac{1}{c^2} \right) - \log \frac{k_l+1}{\delta_n^2} \right) \right) \\ & \leq \sum_{l=0}^L Cnr_l + \sum_{l=0}^L \frac{s_l(k_l+1)}{2} \left\{ -\log \left(\frac{B_l^2}{k_l+1} \left(\frac{1}{t_0 t_0'} + \frac{1}{c^2} \right) \right) + \log((L+1)n) + \sum \log B_m^2 \right\} \\ & \leq \sum_{l=0}^L Cnr_l \end{aligned} \quad (30)$$

where the first inequality follows from (27) and expanding δ_n . The last inequality follows since $n \sum r_l \rightarrow \infty$. Combining (29) and (30) and replacing (28), the proof follows. \blacksquare

Proof of Lemma 11 Condition 2.

$$\text{Assumption : } -\log \lambda_l = O\{(k_l+1)\vartheta_l\}, \quad -\log(1 - \lambda_l) = O\{(s_l/k_{l+1})(k_l+1)\vartheta_l\}$$

Initial parts of proof are same as SS-GL and below is the remaining proof which differs in SS-GHS. Let $\tau_{li}^2 = \beta_{li}\alpha_{li}$, $s^2 = s_a s_b$, $\tau_L^2 = \beta_L \alpha_L$. Thus, $d_{\text{KL}}(q^*, \pi)$ is bounded above by

$$\begin{aligned} & \leq \log \frac{1}{\pi(\mathbf{z}^*)} + \int \int \left[\mathbb{1}(\mathbf{z} = \mathbf{z}^*) \sum_{l,i} \int \int d_{\text{KL}} \left\{ \prod_{l=0}^{L-1} \prod_{i=1}^{k_{l+1}} \prod_{j=1}^{k_l+1} \left\{ z_{li} \mathcal{N}(\bar{w}_{lij}^*, \sigma_i^2) + (1 - z_{li}) \delta_0 \right\} \right. \right. \\ & \left. \left. \prod_{j=1}^{k_L+1} \mathcal{N}(\bar{w}_{Lj}^*, \sigma_L^2) \right\}, \left\{ \prod_{l=0}^{L-1} \prod_{i=1}^{k_{l+1}} \prod_{j=1}^{k_l+1} \left\{ z_{li} \mathcal{N}\left(0, \frac{\sigma_0^2 c^2 \tau_{li}^2 s^2}{c^2 + \tau_{li}^2 s^2}\right) + (1 - z_{li}) \delta_0 \right\} \prod_{j=1}^{k_L+1} \mathcal{N}\left(0, \frac{\sigma_0^2 c^2 \tau_L^2 s^2}{c^2 + \tau_L^2 s^2}\right) \right\} \right. \\ & \quad \left. \times LN(\mu_{li}^{\{\beta\}}, \sigma_{li}^{\{\beta\}2}) LN(\mu_{li}^{\{\alpha\}}, \sigma_{li}^{\{\alpha\}2}) d\beta_{li} d\alpha_{li} \right] LN(\mu^{\{s_b\}}, \sigma^{\{s_b\}2}) LN(\mu^{\{s_a\}}, \sigma^{\{s_a\}2}) ds_b ds_a \\ & + \sum_{l,i} \left[d_{\text{KL}} \left(LN(\mu_{li}^{\{\beta\}}, \sigma_{li}^{\{\beta\}2}), IG\left(\frac{1}{2}, 1\right) \right) + d_{\text{KL}} \left(LN(\mu_{li}^{\{\alpha\}}, \sigma_{li}^{\{\alpha\}2}), \Gamma\left(\frac{1}{2}, 1\right) \right) \right] \\ & + d_{\text{KL}} \left(LN(\mu^{\{s_b\}}, \sigma^{\{s_b\}2}), IG\left(\frac{1}{2}, 1\right) \right) + d_{\text{KL}} \left(LN(\mu^{\{s_a\}}, \sigma^{\{s_a\}2}), \Gamma\left(\frac{1}{2}, s_0^2\right) \right) \\ & = \sum_{l=0}^{L-1} \left(s_l^* \log \frac{1}{\lambda_l} + (k_{l+1} - s_l^*) \log \frac{1}{1 - \lambda_l} \right) \\ & + \sum_{l=0}^{L-1} \sum_{i=1}^{k_{l+1}} \sum_{j=1}^{k_l+1} z_{li}^* \left\{ \frac{1}{2} \log \frac{c^2 \sigma_0^2}{\sigma_i^2} + \frac{(\mu_{li}^{\{\beta\}} + \mu_{li}^{\{\alpha\}} + \mu^{\{s_b\}} + \mu^{\{s_a\}})}{2} - \frac{\log(c^2 + \hat{\beta}_{li} \hat{\alpha}_{li} \hat{s}_b \hat{s}_a)}{2} - \frac{1}{2} \right. \\ & \left. + \frac{\sigma_i^2 + \bar{w}_{lij}^{*2}}{2\sigma_0^2} \left[\exp(-\mu_{li}^{\{\beta\}} - \mu_{li}^{\{\alpha\}} - \mu^{\{s_b\}} - \mu^{\{s_a\}} + \frac{\sigma_{li}^{\{\beta\}2} + \sigma_{li}^{\{\alpha\}} + \sigma^{\{s_b\}2} + \sigma^{\{s_a\}2}}{2}) + \frac{1}{c^2} \right] \right\} \\ & + \sum_{j=1}^{k_L+1} \left\{ \frac{1}{2} \log \frac{c^2 \sigma_0^2}{\sigma_L^2} + \frac{(\mu_L^{\{\beta\}} + \mu_L^{\{\alpha\}} + \mu^{\{s_b\}} + \mu^{\{s_a\}})}{2} - \frac{\log(c^2 + \hat{\beta}_L \hat{\alpha}_L \hat{s}_b \hat{s}_a)}{2} - \frac{1}{2} \right\} \end{aligned}$$

$$\begin{aligned}
& + \frac{\sigma_L^2 + \overline{w}_{Lj}^2}{2\sigma_0^2} \left[\exp(-\mu_L^{\{\beta\}} - \mu_L^{\{\alpha\}} - \mu^{\{s_b\}} - \mu^{\{s_a\}} + \frac{\sigma_L^{\{\beta\}2} + \sigma_L^{\{\alpha\}2} + \sigma^{\{s_b\}2} + \sigma^{\{s_a\}2}}{2}) + \frac{1}{c^2} \right] \Big\} \\
& + \sum_{l=0}^L \sum_{i=1}^{k_{l+1}} \left[\frac{1}{2} \mu_{li}^{\{\beta\}} + \exp\left(-\mu_{li}^{\{\beta\}} + \frac{\sigma_{li}^{\{\beta\}2}}{2}\right) - \log \sigma_{li}^{\{\beta\}} - \log \sqrt{2} - \frac{1}{2} \right] \\
& + \sum_{l=0}^L \sum_{i=1}^{k_{l+1}} \left[-\frac{1}{2} \mu_{li}^{\{\alpha\}} + \exp\left(\mu_{li}^{\{\alpha\}} + \frac{\sigma_{li}^{\{\alpha\}2}}{2}\right) - \log \sigma_{li}^{\{\alpha\}} - \log \sqrt{2} - \frac{1}{2} \right] \\
& + \frac{1}{2} \mu^{\{s_b\}} + \exp\left(-\mu^{\{s_b\}} + \frac{\sigma^{\{s_b\}2}}{2}\right) - \log \sigma^{\{s_b\}} - \log \sqrt{2} - \frac{1}{2} \\
& + \log s_0 - \frac{1}{2} \mu^{\{s_a\}} + \frac{1}{s_0^2} \exp\left(\mu^{\{s_a\}} + \frac{\sigma^{\{s_a\}2}}{2}\right) - \log \sigma^{\{s_a\}} - \log \sqrt{2} - \frac{1}{2} \\
& \leq \sum_{l=0}^{L-1} Cnr_l + \sum_{l=0}^L \frac{s_l^*(k_l+1)}{2} \left\{ (\mu_{li}^{\{\beta\}} + \mu_{li}^{\{\alpha\}} + \mu^{\{s_b\}} + \mu^{\{s_a\}}) + \log \frac{\sigma_0^2}{\sigma_l^2} + \left\{ \frac{\sigma_l^2}{\sigma_0^2} + \frac{B_l^2}{\sigma_0^2(k_l+1)} \right\} \right. \\
& \times \left. \left[\exp\left(-(\mu_{li}^{\{\beta\}} + \mu_{li}^{\{\alpha\}} + \mu^{\{s_b\}} + \mu^{\{s_a\}}) + \frac{\sigma_{li}^{\{\beta\}2} + \sigma_{li}^{\{\alpha\}2} + \sigma^{\{s_b\}2} + \sigma^{\{s_a\}2}}{2}\right) + \frac{1}{c^2} \right] \right\} \\
& - \sum_{l=0}^{L-1} \frac{s_l^*(k_l+1)}{2} \log \left(1 + \frac{\widehat{\beta}_l \widehat{\alpha}_l \widehat{s}_b \widehat{s}_a}{c^2} \right) - \frac{k_L+1}{2} \log \left(1 + \frac{\widehat{\beta}_L \widehat{\alpha}_L \widehat{s}_b \widehat{s}_a}{c^2} \right) \\
& + \sum_{l=0}^L \sum_{i=1}^{k_{l+1}} \left[\frac{1}{2} \mu_{li}^{\{\beta\}} + \exp\left(-\mu_{li}^{\{\beta\}} + \frac{\sigma_{li}^{\{\beta\}2}}{2}\right) - \log \sigma_{li}^{\{\beta\}} - \log \sqrt{2} - \frac{1}{2} \right] \\
& + \sum_{l=0}^L \sum_{i=1}^{k_{l+1}} \left[-\frac{1}{2} \mu_{li}^{\{\alpha\}} + \exp\left(\mu_{li}^{\{\alpha\}} + \frac{\sigma_{li}^{\{\alpha\}2}}{2}\right) - \log \sigma_{li}^{\{\alpha\}} - \log \sqrt{2} - \frac{1}{2} \right] \\
& + \frac{1}{2} \mu^{\{s_b\}} + \exp\left(-\mu^{\{s_b\}} + \frac{\sigma^{\{s_b\}2}}{2}\right) - \log \sigma^{\{s_b\}} - \log \sqrt{2} - \frac{1}{2} \\
& - \frac{1}{2} \mu^{\{s_a\}} + \exp\left(\mu^{\{s_a\}} + \frac{\sigma^{\{s_a\}2}}{2}\right) - \log \sigma^{\{s_a\}} - \log \sqrt{2} - \frac{1}{2}
\end{aligned}$$

The first line follows by Lemma A.4 in Jantre et al. (2022).

We also use $\sum_{j=1}^{k_l+1} \overline{w}_{lij}^2 \leq B_l^2$, (27), $\sigma_0^2 = 1$, $\sigma_l^2 \leq 1$. Further, let $\exp(-\mu_{li}^{\{\beta\}} + \sigma_{li}^{\{\beta\}2}/2) = 1/t_0^2$, $\sigma_{li}^{\{\beta\}2} = 1/\log n$, $\exp(-\mu_{li}^{\{\alpha\}} + \sigma_{li}^{\{\alpha\}2}/2) = t_0$, $\sigma_{li}^{\{\alpha\}2} = 1/\log n$, $\exp(-\mu^{\{s_b\}} + \sigma^{\{s_b\}2}/2) = 1/t_0^2$, $\sigma^{\{s_b\}2} = 1/\log n$. Finally, let $\exp(-\mu^{\{s_a\}} + \sigma^{\{s_a\}2}/2) = t_0$, $\sigma^{\{s_a\}2} = 1/\log n$, then

$$\begin{aligned}
& d_{\text{KL}}(q^*, \pi) \\
& \leq \sum_{l=0}^{L-1} Cnr_l + \sum_{l=0}^L \frac{s_l^*(k_l+1)}{2} \left\{ (\mu_{li}^{\{\beta\}} + \mu_{li}^{\{\alpha\}} + \mu^{\{s_b\}} + \mu^{\{s_a\}}) + \left\{ \sigma_l^2 + \frac{B_l^2}{(k_l+1)} \right\} \right. \\
& \times \left. \left[\exp(-\mu_{li}^{\{\beta\}} - \mu_{li}^{\{\alpha\}} - \mu^{\{s_b\}} - \mu^{\{s_a\}} + \frac{\sigma_{li}^{\{\beta\}2} + \sigma_{li}^{\{\alpha\}2} + \sigma^{\{s_b\}2} + \sigma^{\{s_a\}2}}{2}) + \frac{1}{c^2} \right] - \log \sigma_l^2 \right\} \\
& - \sum_{l=0}^{L-1} \frac{s_l^*(k_l+1)}{2} \log \left(1 + \frac{\widehat{\beta}_l \widehat{\alpha}_l \widehat{s}_b \widehat{s}_a}{c^2} \right) - \frac{k_L+1}{2} \log \left(1 + \frac{\widehat{\beta}_L \widehat{\alpha}_L \widehat{s}_b \widehat{s}_a}{c^2} \right)
\end{aligned}$$

$$\begin{aligned}
& + \sum_{l=0}^L \sum_{i=1}^{k_{l+1}} \left[\frac{1}{2} \mu^{\{\beta\}} + \exp \left(-\mu^{\{\beta\}} + \frac{\sigma_{li}^{\{\beta\}2}}{2} \right) - \log \sigma_{li}^{\{\beta\}} - \log \sqrt{2} - \frac{1}{2} \right] \\
& + \sum_{l=0}^L \sum_{i=1}^{k_{l+1}} \left[-\frac{1}{2} \mu^{\{\alpha\}} + \exp \left(\mu^{\{\alpha\}} + \frac{\sigma_{li}^{\{\alpha\}2}}{2} \right) - \log \sigma_{li}^{\{\alpha\}} - \log \sqrt{2} - \frac{1}{2} \right] \\
& + \frac{1}{2} \mu^{\{s_b\}} + \exp \left(-\mu^{\{s_b\}} + \frac{\sigma^{\{s_b\}2}}{2} \right) - \log \sigma^{\{s_b\}} - \log \sqrt{2} - \frac{1}{2} \\
& - \frac{1}{2} \mu^{\{s_a\}} + \exp \left(\mu^{\{s_a\}} + \frac{\sigma^{\{s_a\}2}}{2} \right) - \log \sigma^{\{s_a\}} - \log \sqrt{2} - \frac{1}{2} \\
& \lesssim \sum_{l=0}^{L-1} Cnr_l + \sum_{l=0}^L \frac{s_l^*(k_l+1)}{2} \left\{ -\log \left(\frac{1}{t_0 t'_0} + \frac{1}{c^2} \right) - \log \sigma_l^2 + \left(1 + \frac{B_l^2}{k_l+1} \right) \left(\frac{1}{t_0 t'_0} + \frac{1}{c^2} \right) \right\} \\
& + \sum_{l=0}^L (k_l+1) \left\{ \log t_0 + \frac{1}{4 \log n} + \frac{1}{t_0^2} + \frac{1}{2} \log(\log n) - \log \sqrt{2} - \frac{1}{2} \right\} \\
& + \sum_{l=0}^L (k_l+1) \left\{ \frac{1}{2} \log t_0 - \frac{1}{4 \log n} + \frac{1}{t_0} + \frac{1}{2} \log(\log n) - \log \sqrt{2} - \frac{1}{2} \right\} \\
& + \left\{ \log t'_0 + \frac{1}{4 \log n} + \frac{1}{t_0'^2} + \frac{1}{2} \log(\log n) - \log \sqrt{2} - \frac{1}{2} \right\} \\
& + \left\{ \frac{1}{2} \log t'_0 - \frac{1}{4 \log n} + \frac{1}{t_0'} + \frac{1}{2} \log(\log n) - \log \sqrt{2} - \frac{1}{2} \right\} \\
& \lesssim \sum_{l=0}^{L-1} Cnr_l + \frac{1}{2} \sum_{l=0}^L s_l^*(k_l+1) \left(-\log \left(\frac{B_l^2}{k_l+1} \left(\frac{1}{t_0 t'_0} + \frac{1}{c^2} \right) \right) + \left(1 + \frac{B_l^2}{k_l+1} \right) \left(\frac{1}{t_0 t'_0} + \frac{1}{c^2} \right) \right) \\
& \qquad \qquad \qquad 2L + 2 \log n + 2 \sum \log B_m \leq \sum_{l=0}^L Cnr_l \quad \blacksquare
\end{aligned}$$

E Additional numerical experiments details

E.1 FLOPs Calculation

We only count multiply operation for floating point operations (FLOPs) similar to Zhao et al. (2019) in ResNet experiments. In 2D convolution layer, we assume convolution is implemented as a sliding window and that the nonlinearity function is computed for free. Then, for a 2D convolutional layer (given bias is present) we have

$$\text{FLOPs} = (C_{in} K_w K_h + 1) O_w O_h C_{out,pruned}$$

where C_{in} is the number of input channels and $C_{out,pruned}$ denotes number of output channels after pruning. Channels are pruned if all the parameters associated with that channel in convolution mapping are zero. K_w and K_h are the kernel width and height respectively. Finally, O_w, O_h are output width and height where $O_w = (I_w + 2 \times P_w - D_w \times (K_w - 1) - 1) / S_w + 1$ and $O_h = (I_h + 2 \times P_h - D_h \times (K_h - 1) - 1) / S_h + 1$. Here, I_w, I_h are input, P_w, P_h are padding, D_w, D_h are dilation, S_w, S_h are stride widths and heights respectively. For fully connected (linear) layers (with bias) we have

$$\text{FLOPs} = (I_{pruned} + 1) O_{pruned}$$

where I_{pruned} and O_{pruned} are number of pruned input and output neurons.

E.2 Variational parameters initialization

We initialize γ_{lj} 's close to 1. This ensures that at epoch 0, we have a fully connected network. The variational parameters $\mu_{ljj'}$ are initialized using Kaiming uniform initialization (He et al., 2015). We reparameterize $\sigma_{ljj'}$ with softplus function: $\sigma_{ljj'} = \log(1 + \exp(\rho_{ljj'}))$ and initialize $\rho_{ljj'}$ to -6. Thus, initial values of $\sigma_{ljj'}$ are close to 0 ensuring that initial values of network weights stay close to Kaiming uniform initialization.

In SS-GL, $\mu_{lj}^{\{\tau\}}$ is initialized with $U(-0.6, 0.6)$ and $\sigma_{lj}^{\{\tau\}} = \log(1 + \exp(\rho_{lj}^{\{\tau\}}))$ where $\rho_{lj}^{\{\tau\}}$ are initialized to -6. Further, μ_{ζ} is initialized to 1 and $\sigma_{\zeta} = \log(1 + \exp(\rho^{\{\tau\}}))$ where $\rho^{\{\tau\}}$ is initialized to -6. In SS-GHS, both $\mu_{lj}^{\{\alpha\}}$ and $\mu_{lj}^{\{\beta\}}$ are initialized with $U(-0.6, 0.6)$. Also, $\sigma_{lj}^{\{\alpha\}} = \log(1 + \exp(\rho_{lj}^{\{\alpha\}}))$ and $\sigma_{lj}^{\{\beta\}} = \log(1 + \exp(\rho_{lj}^{\{\beta\}}))$ where $\rho_{lj}^{\{\alpha\}}$ and $\rho_{lj}^{\{\beta\}}$ initialized to -6. Moreover, $\mu^{\{s_a\}}$ and $\mu^{\{s_b\}}$ are initialized to 1. Lastly $\sigma^{\{s_a\}} = \log(1 + \exp(\rho^{\{s_a\}}))$ and $\sigma^{\{s_b\}} = \log(1 + \exp(\rho^{\{s_b\}}))$ where $\rho^{\{s_a\}}$, $\rho^{\{s_b\}}$ are initialized to -6.

E.3 Hyperparameters for training

In MLP-MNIST and LeNet-5-Caffe-MNIST, we use 10^{-3} learning rate and 1024 minibatch size for all three models (SS-IG, SS-GL SS-GHS). In LeNet-5-Caffe-Fashion-MNIST experiment, we use minibatch size of 1024 and learning rates of 2×10^{-3} , 1×10^{-3} , 2×10^{-3} for SS-IG, SS-GL and SS-GHS respectively. For MLP and LeNet-5-Caffe experiments, we train all the models until 1200 epochs using Adam optimizer.

References

- Jose M Alvarez and Mathieu Salzmann. Learning the number of neurons in deep networks. In Proceedings of the 30th Advances in Neural Information Processing Systems (NIPS 2016), Barcelona, Spain, 2016.
- A. Armagan, D. B. Dunson, J. Lee, W. U. Bajwa, and N. Strawn. Posterior consistency in linear models under shrinkage priors. Biometrika, 100(4):1011–1018, 2013. ISSN 00063444.
- Jincheng Bai, Qifan Song, and Guang Cheng. Efficient variational inference for sparse deep learning with theoretical guarantee. In Proceedings of the 34th Advances in Neural Information Processing Systems (NeurIPS 2020), pages 466–476, Vancouver, Canada, 2020.
- Ray Bai and Malay Ghosh. High-dimensional multivariate posterior consistency under global–local shrinkage priors. Journal of Multivariate Analysis, 167:157–170, 2018. ISSN 0047-259X.
- Michael Betancourt and Mark Girolami. Hamiltonian monte carlo for hierarchical models. Current trends in Bayesian methodology with applications, 79(30), 2015.
- Anindya Bhadra, Jyotishka Datta, Nicholas G. Polson, and Brandon T. Willard. Lasso meets horseshoe: A survey. Statistical Science, 34(3):405–427, 2019.
- David M. Blei and John D. Lafferty. A correlated topic model of science. The Annals of Applied Statistics, 1(1):17–35, 2007.
- David M. Blei, Alp Kucukelbir, and Jon D. McAuliffe. Variational inference: A review for statisticians. Journal of the American Statistical Association, 112(518):859–877, 2017. ISSN 1537-274X.
- Charles Blundell, Julien Cornebise, Koray Kavukcuoglu, and Daan Wierstra. Weight uncertainty in neural network. In Proceedings of Machine Learning Research, volume 37, pages 1613–1622. PMLR, 2015.

- Yu Cheng, Duo Wang, Pan Zhou, and Tao Zhang. Model compression and acceleration for deep neural networks: The principles, progress, and challenges. IEEE Signal Processing Magazine, 35(1):126–136, 2018.
- Badr-Eddine Chérif-Abdellatif. Convergence rates of variational inference in sparse deep learning. In Proceedings of the 37th International Conference on Machine Learning (ICML-2020), volume 119, pages 1831–1842, Vienna, Austria, 2020.
- Stefan Elfving, Eiji Uchibe, and Kenji Doya. Sigmoid-weighted linear units for neural network function approximation in reinforcement learning. Neural Networks, 107:3–11, 2018. ISSN 0893-6080. Special issue on deep reinforcement learning.
- Jonathan Frankle and Michael Carbin. The lottery ticket hypothesis: Finding sparse, trainable neural networks. In International Conference on Learning Representations (ICLR 2019), New Orleans, USA, 2019.
- Jerome Friedman, Trevor Hastie, and Robert Tibshirani. The elements of statistical learning. Springer series in statistics. Springer, New York, 2009.
- Trevor Gale, Erich Elsen, and Sara Hooker. The state of sparsity in deep neural networks. arXiv:1902.09574, 2019.
- Soumya Ghosh, Jiayu Yao, and Finale Doshi-Velez. Model selection in bayesian neural networks via horseshoe priors. Journal of Machine Learning Research, 20:1–46, 2019.
- Yiwen Guo, Anbang Yao, and Yurong Chen. Dynamic network surgery for efficient dnns. In D. Lee, M. Sugiyama, U. Luxburg, I. Guyon, and R. Garnett, editors, Proceedings of the 29th Advances in Neural Information Processing Systems (NIPS 2016), volume 29, 2016.
- Song Han, Jeff Pool, John Tran, and William Dally. Learning both weights and connections for efficient neural network. In Proceedings of the 28th Advances in Neural Information Processing Systems (NIPS 2015), volume 28, 2015.
- Kaiming He, Xiangyu Zhang, Shaoqing Ren, and Jian Sun. Delving deep into rectifiers: Surpassing human-level performance on imagenet classification. In IEEE International Conference on Computer Vision (ICCV-2015), pages 1026–1034, 2015.
- Kaiming He, Xiangyu Zhang, Shaoqing Ren, and Jian Sun. Deep residual learning for image recognition. In IEEE Conference on Computer Vision and Pattern Recognition (CVPR-2016), pages 770–778, 2016.
- Geoffrey E Hinton and Drew Van Camp. Keeping the neural networks simple by minimizing the description length of the weights. In Proceedings of the sixth annual conference on Computational Learning Theory (COLT-1993), page 5–13, Santa Cruz, USA, 1993.
- John B Ingraham and Debora S Marks. Variational inference for sparse and undirected models. In International Conference on Machine Learning (ICML), 2017.
- Pavel Izmailov, Sharad Vikram, Matthew D Hoffman, and Andrew Gordon Gordon Wilson. What are bayesian neural network posteriors really like? In Proceedings of the 38th International Conference on Machine Learning (ICML-2021), pages 4629–4640, 2021.
- Eric Jang, Shixiang Gu, and Ben Poole. Categorical reparameterization with gumbel-softmax. In 5th International Conference on Learning Representations (ICLR 2017), Toulon, France, 2017.

- Sanket Jantre, Shrijita Bhattacharya, and Tapabrata Maiti. Layer adaptive node selection in bayesian neural networks: Statistical guarantees and implementation details. [arXiv:2108.11000](https://arxiv.org/abs/2108.11000), 2022.
- Michael I. Jordan, Zoubin Ghahramani, Tommi S. Jaakkola, and Lawrence K. Saul. An introduction to variational methods for graphical models. *Machine Learning*, 37:183–233, 1999.
- Zhuang Liu, Jianguo Li, Zhiqiang Shen, Gao Huang, Shoumeng Yan, and Changshui Zhang. Learning efficient convolutional networks through network slimming. In *Proceedings of the IEEE International Conference on Computer Vision (ICCV)*, 2017.
- Christos Louizos, Karen Ullrich, and Max Welling. Bayesian compression for deep learning. In *Proceedings of the 30th Advances in Neural Information Processing Systems (NIPS 2020)*, pages 3288–3298, Long Beach, CA, USA, 2017.
- Christos Louizos, Max Welling, and Diederik P. Kingma. Learning sparse neural networks through l_0 regularization. In *International Conference on Learning Representations*, 2018.
- Lu Lu, Yeonjong Shin, Yanhui Su, and George Em Karniadakis. Dying relu and initialization: Theory and numerical examples. *Communications in Computational Physics*, 28(5):1671–1706, 2020.
- Jian-Hao Luo, Jianxin Wu, and Weiyao Lin. Thinet: A filter level pruning method for deep neural network compression. In *Proceedings of the IEEE International Conference on Computer Vision (ICCV)*, 2017.
- Chris J. Maddison, Andriy Mnih, and Yee Whye Teh. The concrete distribution: A continuous relaxation of discrete random variables. In *5th International Conference on Learning Representations (ICLR 2017)*, Toulon, France, 2017.
- T. J. Mitchell and J. J. Beauchamp. Bayesian variable selection in linear regression. *Journal of the American Statistical Association*, 83(404):1023–1032, 1988.
- Dmitry Molchanov, Arsenii Ashukha, and Dmitry Vetrov. Variational dropout sparsifies deep neural networks. In *Proceedings of the 34th International Conference on Machine Learning (ICML-2027)*, volume 70, page 2498–2507, Sydney, NSW, Australia, 2017.
- Kenton Murray and David Chiang. Auto-sizing neural networks: With applications to n-gram language models. In *Proceedings of the 2015 Conference on Empirical Methods in Natural Language Processing (EMNLP 2015)*, pages 908–916, Lisbon, Portugal, 2015.
- Tsubasa Ochiai, Shigeki Matsuda, Hideyuki Watanabe, and Shigeru Katagiri. Automatic node selection for deep neural networks using group lasso regularization. *CoRR*, abs/1611.05527, 2016.
- Adam Paszke, Sam Gross, Francisco Massa, Adam Lerer, James Bradbury, Gregory Chanan, Trevor Killeen, Zeming Lin, Natalia Gimelshein, Luca Antiga, Alban Desmaison, Andreas Kopf, Edward Yang, Zachary DeVito, Martin Raison, Alykhan Tejani, Sasank Chilamkurthy, Benoit Steiner, Lu Fang, Junjie Bai, and Soumith Chintala. Pytorch: An imperative style, high-performance deep learning library. In *Advances in Neural Information Processing Systems 32*, pages 8024–8035. Curran Associates, Inc., 2019.
- Juho Piironen and Aki Vehtari. On the hyperprior choice for the global shrinkage parameter in the horseshoe prior. In *Conference on Artificial Intelligence and Statistics (AISTATS)*, 2017.
- N. Polson and V. Ročková. Posterior concentration for sparse deep learning. In *32nd Conference on Advances in Neural Information Processing Systems (NeurIPS 2018)*, pages 930–941, Montréal, Canada, 2018.

- Prajit Ramachandran, Barret Zoph, and Quoc V. Le. Searching for activation functions. CoRR, abs/1710.05941, 2017.
- J. Schmidt-Hieber. Nonparametric regression using deep neural networks with relu activation function. The Annals of Statistics, 48(4):1875–1897, 2020.
- Yan Sun, Qifan Song, and Faming Liang. Consistent sparse deep learning: Theory and computation. Journal of the American Statistical Association, 0(ja):1–42, 2021.
- Ilya Sutskever, James Martens, George Dahl, and Geoffrey Hinton. On the importance of initialization and momentum in deep learning. In Proceedings of the 30th International Conference on Machine Learning (ICML-2013), volume 28, pages 1139–1147, 2013.
- Wei Wen, Chunpeng Wu, Yandan Wang, Yiran Chen, and Hai Li. Learning structured sparsity in deep neural networks. In Proceedings of the 29th Advances in Neural Information Processing Systems (NIPS 2016), Barcelona, Spain, 2016.
- Andrew G Wilson and Pavel Izmailov. Bayesian deep learning and a probabilistic perspective of generalization. Advances in neural information processing systems, 33:4697–4708, 2020.
- Xiaofan Xu and Malay Ghosh. Bayesian variable selection and estimation for group lasso. Bayesian Analysis, 10(4):909–936, 2015.
- Chenglong Zhao, Bingbing Ni, Jian Zhang, Qiwei Zhao, Wenjun Zhang, and Qi Tian. Variational convolutional neural network pruning. In 2019 IEEE/CVF Conference on Computer Vision and Pattern Recognition (CVPR), pages 2775–2784, 2019.
- Zhun Zhong, Liang Zheng, Guoliang Kang, Shaozi Li, and Yi Yang. Random erasing data augmentation. Proceedings of the AAAI Conference on Artificial Intelligence, 34(07):13001–13008, 2020.
- Michael Zhu and Suyog Gupta. To prune, or not to prune: Exploring the efficacy of pruning for model compression. In 6th International Conference on Learning Representations (ICLR 2018), Workshop Track Proceedings, Vancouver, Canada, 2018. OpenReview.net.